



Power-law scaling behavior of A-phase events during sleep: Normal and pathologic conditions

Martin O. Mendez^a, J.S. Murguía^b, Alfonso Alba^{b,*}, V.E. Arce-Guevara^b,
H. González-Aguilar^b, Guillermina Guerrero-Mora^c

^a Laboratorio Nacional Centro de Investigación en Imagenología e Instrumentación Médica, Facultad de Ciencias & CICSaB, Universidad Autónoma de San Luis Potosí, Mexico

^b Laboratorio Nacional Centro de Investigación en Imagenología e Instrumentación Médica, Facultad de Ciencias, Universidad Autónoma de San Luis Potosí, Mexico

^c Unidad Académica Multidisciplinaria Zona Media, Universidad Autónoma de San Luis Potosí, Mexico

ARTICLE INFO

Article history:

Received 28 May 2019

Received in revised form 11 October 2019

Accepted 8 November 2019

Available online 22 November 2019

Keywords:

Cyclic alternating pattern

DFA

CAP

Self-affine process

Long-range dependence

ABSTRACT

Objective: A-phases are short-time cortical events during sleep that repeatedly disrupt the basal fluctuations of electrical brain activity. They are the basic units of the cyclic alternating pattern (CAP), which is related to the instability and consolidation of the sleep process. The main purpose of this study is to evaluate the temporal occurrence of A-phases (TOAP) under normal and pathologic sleep conditions.

Methods: To derive a quantitative description of TOAP, we have applied detrended fluctuation analysis (DFA), to unveil scale-free behavior from non-stationary time series. Data from sleep recordings of 15 healthy subjects (H), 37 with nocturnal frontal lobe epilepsy (NFLE), 9 with periodic leg movement (PLM), and 22 with REM Sleep Behavior Disorder (RBD) from the Physionet database were used. TOAP was computed from binary time series constructed from A-phase annotations, where symbols 1 and -1, represent the presence or absence of an A-phase, respectively. These time series were analyzed through DFA and characterized by the scaling exponent.

Results: In all cases, numerical results show evidence that a statistical fractal structure is embedded in TOAP, where persistent scaling behavior is observed with scaling exponent close to 1.

Conclusion: The sleep process maintains a similar structure from the A-phase perspective despite of internal or external factors that could affect the sleep process, suggesting that sleep may be a resilient process.

Significance: The scaling exponent of the A-phase occurrence provides new information about the sleep process that may have clinical relevance and complementary to standard clinical indices such as the CAP-rate.

© 2019 Elsevier Ltd. All rights reserved.

1. Introduction

Biological systems exhibit a complex, non-stationary and non-linear behavior. However, this behavior could be largely affected by stress and diseases that affect the structural and temporal complexity of the system towards a more predictable behavior. Some examples of these modifications have been found in lung architecture [1], stride rate fluctuations [2], heart rate fluctuations [3], behavioral complexity [4], plant branch architecture [5], and electrical activity of the brain during sleep [6]. Therefore, a complex behavior in biological systems seems to be a fundamental char-

acteristic for adaptability facilitating the reaction to unpredictable situations that can damage the system [7,8].

It is well known that many complex systems present the self-affinity property, which is related to fractal structures. For self-affine systems, the statistical distribution of the measured quantity follows a power-law function, which is a mathematical function without a characteristic scale. Thus, self-affine phenomena are called scale-free [9]. Scale-free behavior reflects a tendency of complex systems to develop correlations that decay slowly and extend over large distance in time or space. Since the later behavior cannot be assumed a priori, then it has to be established. Hence, robust analysis techniques are needed to differentiate truly scale-free behavior from mock behavior produced, e.g., by non-stationarities in the data, which are a major problem for the characterization of the scaling properties of the data [10]. At the present time,

* Corresponding author.

E-mail address: fac@fc.uaslp.mx (A. Alba).

Introducing supersymmetric quantum mechanics via point canonical transformations

Gabriel González^{1,2,*}

¹*Cátedra CONCAYT, Universidad Autónoma de San Luis Potosí, San Luis Potosí, 78000 MEXICO*

²*Coordinación para la Innovación y la Aplicación de la Ciencia y la Tecnología, Universidad Autónoma de San Luis Potosí, San Luis Potosí, 78000 MEXICO*

(Dated: February 6, 2023)

We propose an alternative way to introduce supersymmetric quantum mechanics to physics students using a point canonical coordinate transformation. We provide two point canonical transformations that allow us to obtain new supersymmetric partner Hamiltonians with iso-spectral and non iso-spectral energy eigenvalues starting from a known solvable Hamiltonian. We illustrate this new approach by applying it to the harmonic oscillator potential.

PACS numbers: 03.65.-w, 03.65.Fd, 03.65.Ge

Keywords: Supersymmetric quantum mechanics, Point canonical transformations, Schrödinger equation

I. INTRODUCTION

The dynamics of quantum mechanical systems is determined by solving the time dependent Schrödinger equation which is written in operator form as¹

$$i\hbar \frac{d}{dt} |\psi(t)\rangle = \hat{H} |\psi(t)\rangle, \quad (1)$$

where $\hat{H} = \hat{p}^2/2m + U(x, t)$ represents the Hamiltonian of the system and $U(x, t)$ represents the potential energy of the system. For the case when the potential energy of the system is time independent one is primarily interested in finding the eigenvalues and eigenfunctions of the eigenvector equation $\hat{H} |\psi_n\rangle = \mathcal{E}_n |\psi_n\rangle$, which assumes the following differential equation form with respect to the position basis²

$$-\frac{\hbar^2}{2m} \frac{d^2 \psi_n(x)}{dx^2} + U(x) \psi_n(x) = \mathcal{E}_n \psi_n(x). \quad (2)$$

Generations of physicists have been trained to solve Eq. (2) for a few exactly solvable potentials by using a handful of mathematical techniques which include power series solutions, integral transforms, raising and lowering operators, and often finding solutions in terms of special functions.³ Exact solutions to the non relativistic Schrödinger equation are important because they often reveal the underlying symmetry and invariance of the physical system. It is therefore essential to develop special techniques to obtain exact solutions to the non relativistic Schrödinger equation.

The number of known exactly solvable quantum potentials has expanded considerably in recent years due to supersymmetric (SUSY) quantum mechanics.⁴ SUSY quantum mechanics is based on the factorization method first proposed by Dirac in 1930 in order to solve the one dimensional harmonic oscillator.⁵⁻⁷ A decade later, Infeld and Hull gave a classification of all systems solvable through the factorization method.⁸⁻¹⁰

Supersymmetry was proposed in 1981 by Witten in order to find an underlying structure for the fundamental forces of nature.^{11,12} Soon, the ideas of supersymmetry led to new approaches to other areas of physics like atomic, molecular, nuclear, optical and condensed matter physics as well as non

relativistic quantum mechanics. In Witten's one dimensional SUSY quantum mechanics the Hamiltonian of a given system is represented by a pair of SUSY partner Hamiltonians H_{\pm} for which the energy of the ground state for H_{-} is set to zero. Apart from the ground state of H_{-} , the energy levels of H_{\pm} are iso-spectral, SUSY is said to be broken in the case when a zero energy state does not exist. The energy states of the two partner Hamiltonians are related by first order differential operators through the so called intertwining relations. This procedure allow us to generate new solvable potentials starting from a known solution.^{13,14}

In 1983 Gendenshtein introduced the concept of *shape invariance*, where he showed that the eigenfunctions and eigenvalues could be obtained algebraically whenever a parametric relation is satisfied by the two supersymmetric partner Hamiltonians without knowing a priori the spectrum of its partner.¹⁵ In 1984 Mielnik showed that there exists a family of equivalent partner Hamiltonians and obtained a family of quantum potentials iso-spectral to the harmonic oscillator.¹⁶⁻²¹

Another method that yields new exactly solvable potentials that is not related with the factorization method and supersymmetry is the so called operator transformation method.²²⁻²⁴ The operator transformation procedure was used by Natanzon who applied it to transform the Schrödinger equation into the hypergeometric and the confluent hypergeometric differential equation.²⁵⁻²⁷

There are also other type of transformations called point canonical transformations (PCT) which transform a Schrödinger type equation into a known Schrödinger equation so that the solution is obtained through the known solution.²⁸⁻³² Our main goal is to apply two different PCTs to the Schrödinger equation which give iso-spectral and non-iso-spectral eigenvalues for the harmonic oscillator potential. We obtain two pairs of SUSY partner Hamiltonians whose eigenfunctions are related by first order differential operators, therefore, the resulting PCT will interrelate Schrödinger's and Witten's Hilbert spaces and will give the energy spectrum and eigenfunctions in terms of the usual SUSY algebra.

The article is organized as follows, in the following section we apply a PCT on Schrödinger's equation and obtain the necessary conditions over which a PCT gives us a SUSY quantum mechanical structure. In next section we demonstrate the util-

Electroluminescent characterization of commercial solar panels.

Lorena Rodríguez Salas*, Oscar F. Núñez Olvea, Alfonso Lastras Martínez,

Instituto de Investigación en Comunicación Óptica de la Universidad Autónoma de San Luis Potosí. IICO-UASLP
San Luis Potosí, S.L.P., México

Electroluminescence (EL) has become a very convenient tool to evaluate the quality of Si solar panels. The EL emission in a directly polarized p-n junction is generated by the recombination of minority carriers injected into the neutral regions adjacent to the junction. In comparison to direct gap materials like GaAs, the electroluminescent emission of Si is weak due to its indirect band gap nature. It is, nevertheless, measurable with infrared detectors sensitive to wavelengths around the band gap of Si (1.15 μm), including CCD cameras.

Fuyuki et al obtained EL images of a polycrystalline Silicon cell and found a linear relationship between the intensity of the EL emission and the diffusion length of minority carriers [1]. Because of its indirect band gap, the lifetime of minority carriers in Silicon is dominated by recombination through deep levels (Shockley-Read-Hall recombination). The concentration of deep levels is thus directly related to the local diffusion length and a map of the EL intensity across the cell surface would give a measure of cell uniformity and cell quality.

Here, we report on EL images of multicrystalline and monocrystalline Si commercial panels (**fabricante y potencia**). Such images were obtained with a commercial photographic camera (**fabricante**) by removing its infrared filter to enhance IR sensitivity. These images are of good quality and allow us to evaluate the homogeneity of the p-n union of a cell, as well to map the distribution of crystalline defects across the cells that comprise the solar panel.

Our results indicate that it is possible to obtain EL images of solar panels of good quality employing instrumentation with a moderate cost. This makes the technique affordable for an ample range of applications, including the quick characterization of commercial panels. It also allows its use in teaching laboratories for didactic purposes.

Keywords: EL; Electroluminescence imaging; Solar cells; PV modules; Crystalline defects

1. Introduction

High quality, high yield and maximum power output are crucial objectives for solar cell manufacturers and customers at the same time. Solar cells are large-area diodes optimized for light absorption and charge carrier collection. Inverting the normal operating mode by injecting charge carrier under applied forward bias leads to recombination in the device. Although most solar cells are not particularly efficient light emitters, part of the recombination will be radiative, leading to detectable emission of photons with energies around the band gap of the solar-cell absorber.[6]

In comparison to energetic-breached direct material, like GaAs, the electroluminescence of Si is low due to its indirect band gap nature, nevertheless, it is measurable with a photographic camera adapted to work in near infrared, and with a sufficiently integration time.

Fuyuki et al obtained images of electroluminescence (EL) in a polycrystalline silicon cell, and they found a linear relation between the intensity of the luminescence and the diffusion length of minority carriers. [1] This is because the indirect nature of the prohibited breach of silicon makes that life span of carriers, which determine the diffusion length, is in its turn determined by the recombination throughout flaws. In that way, as the number of flaws rises, the life span reduces, and with this, the intensity of the luminescence and diffusion length.

Here, we report on EL images of polycrystalline and monocrystalline Si commercial solar panels (polycrystalline panels Solartec 250 W, Solarnorte 265 W, Canadian Solar 250 W and monocrystalline Q Cells panels 370 W). These images were obtained with a commercial photographic camera (EOS 50D Canon) by removing its infrared filter to enhance IR sensitivity. Good quality images allow us to evaluate the homogeneity of the p-n union of a cell, as well to map the distribution of crystalline defects across the cells that comprise the solar panel.

2. Electroluminescence basics

EL, that is, the emission of light in consequence to the application of a forward voltage bias to a diode, is the reciprocal action to the standard operation of a solar cell, namely the conversion of incident light electricity. According to the reciprocity theorem, the EL intensity Φ_{em} of a p-n-junction solar cell emitted at any position $r=(x,y)$ of the solar-cell surface is given by [2].

$$\begin{aligned}\Phi_{em}(E, r) &= [1 - R(E, r)]Q_i(E, r)\Phi_{bb}(E)\exp\left(\frac{qV(r)}{kT}\right) \\ &= Q_e(E, r)\Phi_{bb}(E)\exp\left(\frac{qV(r)}{kT}\right)\end{aligned}$$

Where kT/q is the thermal voltage, $V(r)$ is the internal junction voltage, E is the photon energy, and $Q_e(r) = [1 - R(r)]Q_i(r)$ is the local external quantum efficiency



Thermal impedance analysis of nano-dipole linear arrays for energy harvesting applications



Brhayllan Mora-Ventura^{a,b,*}, John Eder Sánchez^a, Gabriel González^a, Francisco J. González^a

^a Universidad Autónoma de San Luis Potosí, Sierra Leona, 550, Lomas 2da Sección, Building CIACYT, 78210 San Luis Potosí, Mexico

^b Universidad Marista de San Luis Potosí, Beato Marcelino Champagnat, 305, 78413 San Luis Potosí, S.L.P., Mexico

ARTICLE INFO

Keywords:

Thermal impedance
Nanoarrays
Thermoelectric
Nanostructures

ABSTRACT

Efficient thermal harvesting energy applications, based on the Seebeck effect, require systems with high thermal impedance to enhance both the thermal and electric response. In this work, we study the thermal impedance (Z_{th}) response on steady conditions of metal dipole nanoarrays fabricated on polyimide and silicon dioxide (SiO_2) substrates by electron beam lithography. The experimental thermal characteristics of the nanoarray, measured with a thermal camera, reveals a high delta temperature of 89.8 °C and a high thermal impedance of 292.2 (K/W) in polyimide, in contrast with the ones obtained in SiO_2 , which were around 63.9 °C and 13.5 (K/W), respectively. In addition, numerical simulations were performed using COMSOL multi-physics software. The numerical results support a higher thermal impedance in polyimide than the one for SiO_2 . These results show that polyimide could be a better thermal responsive substrate for thermal harvesting energy applications compared with its counterpart fabricated on SiO_2 .

1. Introduction

The harvesting of thermal and electromagnetic radiation has gained a lot of attention during the last decades in fields such as: opto-electronics, nano-generators, and thermoelectric devices [1,2]. For instance, the need of thermal harvesting applications to convert thermal waste dissipation into useful electrical current has increased due to the availability of power waste in thermal-solar cells and photovoltaic cells. Several studies have shown that the thermal dissipation response depends on several parameters such as: temperature, substrate material, morphology and dimensions.

More recently, some reports are focused on the heat transfer problems that appear due to the performance on thermal substrates [3–5]. For example, in the last decade, thermoelectric nanoantennas, also known as Seebeck nanoantennas (capturing energy of free-propagating infrared waves, turning them into induced current), have been successfully used as energy harvesters because their tunability and possibility of collecting the longest wavelengths of the solar spectrum, which make them useful to convert the thermal energy waste into electricity through the Seebeck effect. Additionally, during the conversion process, an increase in temperature is generated that could be converted into an electric potential through the Seebeck effect [6]. Nowadays, theoretical and experimental efforts in thermoelectric applications have contributed to enhance the performance and achieved high-efficiencies

using different geometries, materials and substrates [7,8]. Indeed, a significant experimental improvement in the efficiency of nanostructured thermoelectric devices could be achieved by increasing their thermal insulation properties. For example, Szakmany et al. described nano-devices fabricated on silicon substrates with a silicon dioxide (SiO_2) layer for the study of thermal and electrical insulation. In fact, they have shown that a SiO_2 layer acts as a thermal insulator allowing the structures to reach higher temperature gradients [2,9–12]. Therefore, the use of flexible polymers has been proposed to improve the thermal insulation of thermoelectric devices. For example, polymers such as polyimide (PI) has the advantage, when used as a substrate, of being flexible, lightweight, with high temperature resistance and low thermal expansion coefficient, among other characteristics [13–17].

It is widely understood that thermal impedance studies require the use of heat transfer theory including: conduction, radiation, convection and transient thermal impedance in steady conditions. Therefore, to describe the physics involved in thermal transport phenomena, it is necessary to consider how geometry, power dissipation and time affect to the temperature distribution.




In this study we report the thermal impedance analysis of thermal dipole nanoarrays fabricated on flexible (polyimide) and hard substrates (silicon wafer with a 300 nm SiO_2 layer). The study includes; thermal experiments by using an in-plane thermal camera (Optotherm EL InfraSight 320) as well as numerical simulations using COMSOL

* Corresponding author.

A wide band porous silicon omnidirectional mirror for the near infrared range

Cite as: J. Appl. Phys. **127**, 203106 (2020); <https://doi.org/10.1063/1.5144621>

Submitted: 08 January 2020 . Accepted: 06 May 2020 . Published Online: 27 May 2020

B. A. Chavez-Castillo , J. S. Pérez-Huerta , J. Madrigal-Melchor , S. Amador-Alvarado , I. A. Sustaita-Torres , V. Agarwal , and D. Ariza-Flores 



ARTICLES YOU MAY BE INTERESTED IN

[Precise measurement of the temperature of a silicon wafer by an optical-interference contactless thermometer during rapid plasma processing](#)

Journal of Applied Physics **127**, 203302 (2020); <https://doi.org/10.1063/1.5143834>

[Temporal differential elastic wave computational metamaterials](#)

Journal of Applied Physics **127**, 203104 (2020); <https://doi.org/10.1063/5.0003973>

[Dark current analysis of germanium-on-insulator vertical p-i-n photodetectors with varying threading dislocation density](#)

Journal of Applied Physics **127**, 203105 (2020); <https://doi.org/10.1063/5.0005112>

Lock-in Amplifiers
up to 600 MHz





Effective control of biofilms by photothermal therapy using a gold nanorod hydrogel

Carlos Bermúdez-Jiménez¹ | Nereyda Niño-Martínez² | Nuria Patiño-Marín¹ | Fidel Martínez-Gutiérrez³ | Facundo Ruiz² | Horacio Bach⁴ | Gabriel Martínez-Castañón¹

¹Laboratorio de Nanobiomateriales, Facultad de Estomatología, Universidad Autónoma de San Luis Potosí, San Luis Potosí, Mexico

²Facultad de Ciencias, Universidad Autónoma de San Luis Potosí, San Luis Potosí, Mexico

³Facultad de Ciencias Químicas, Universidad Autónoma de San Luis Potosí, San Luis Potosí, Mexico

⁴Department of Medicine, Division of Infectious Diseases, University of British Columbia, Vancouver, British Columbia, Canada

Correspondence

Gabriel Martínez-Castañón, Laboratorio de Nanobiomateriales, Facultad de Estomatología, Universidad Autónoma de San Luis Potosí, Av. Dr. Manuel Nava No. 2, Zona Universitaria, San Luis Potosí, C.P. 78290, Mexico.
Email: mtzcastanon@fciencias.uaslp.mx

Funding information

Consejo Nacional de Ciencia y Tecnología, Grant/Award Number: Scholarship Number 695756

Abstract

Biofilms are matrices synthesized by bacteria containing polysaccharides, DNA, and proteins. The development of biofilms in infectious processes can induce a chronic inflammatory response that may progress to the destruction of tissues. The treatment of biofilms is difficult because they serve as a bacterial mechanism of defense and high doses of antibiotics are necessary to treat these infections with limited positive results. It has been demonstrated that photothermal therapy using gold nanorods (AuNRs) is an attractive treatment because of its anti-biofilm activity. The purpose of this work was to generate a novel chitosan-based hydrogel embedded with AuNRs to evaluate its anti-biofilm activity. AuNRs were synthesized by the seed-mediated growth method and mixed with the chitosan-based hydrogel. Hydrogels were characterized and tested against two bacterial strains by irradiating the produced biofilm in the presence of the nanoformulation with a laser adjusted at the near infrared spectrum. In addition, the safety of the nanoformulation was assessed with normal human gingival fibroblasts. Results showed that a significant bacterial killing was measured when biofilms were exposed to an increase of 10°C for a short time of 2 min. Moreover, no cytotoxicity was measured when normal gingival fibroblasts were exposed to the nanoformulation using the bactericidal conditions. The development of the reported formulation can be used as a direct application to treat periodontal diseases or biofilm-produced bacteria that colonize the oral cavity.

KEYWORDS

biofilm, chitosan, *E faecalis*, gingival fibroblasts, gold nanorods, photothermal therapy, *S oralis*

1 | INTRODUCTION

Biofilms are complex communities of microorganisms embedded in a large and highly hydrated matrix of exopolysaccharides (EPS), which are attached to an inert solid surface or a living tissue. The development of biofilms poses a challenge because of the elevated doses of antibiotics necessary to eradicate them. Moreover, biofilms facilitate the development of bacteria due to the communication between the

population's quorum sensing (De Sordi & Mühlischlegel, 2009; Waters & Bassler, 2005).

The oral cavity represents a perfect niche for the development of biofilms because of the ideal conditions of temperature, nutrient supply, and proper surfaces for the adhesion of bacteria. The formation and persistence of biofilms may induce a focal and chronic inflammatory response by the host, leading to the destruction of the supporting tissues of the tooth (Siqueira, Rôças, Alves, & Silva, 2009). Current

Potential of Mean Force Calculations for an S_N2 Fluorination Reaction in Five Different Imidazolium Ionic Liquid Solvents Using Quantum Mechanics/Molecular Mechanics Molecular Dynamics Simulations

Joel Sánchez-Badillo, Marco Gallo,* Ricardo A. Guirado-López, and Raúl González-García

Cite This: *J. Phys. Chem. B* 2020, 124, 4338–4357

Read Online

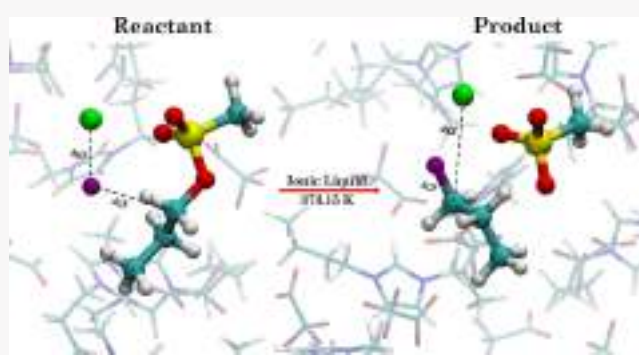
ACCESS |

Metrics & More

Article Recommendations

Supporting Information

ABSTRACT: The use of ionic liquids (ILs) as both catalysts and solvents in a wide range of chemical reactions has received considerable attention over the last few years due to their positive effects in enhancing reaction rates and selectivities. In this work, hybrid quantum mechanics/molecular mechanics (QM/MM) molecular dynamics simulations were carried out in conjunction with umbrella-sampling techniques to study the bimolecular nucleophilic substitution (S_N2) fluorination reaction between propyl-mesylate and potassium fluoride using five ILs as solvents, specifically, 1-butyl-3-methylimidazolium mesylate ($[C_4mim][OMs]$), 1-butyl-3-methylimidazolium tetrafluoroborate ($[C_4mim][BF_4]$), 1-butyl-3-methylimidazolium trifluoroacetate ($[C_4mim][CF_3COO]$), 1-butyl-3-methylimidazolium bromide ($[C_4mim][Br]$), and 1-butyl-3-methylimidazolium chloride ($[C_4mim][Cl]$) at 373.15 K. The QM region (reactive part) in all QM/MM systems was simulated using the Parametric Method 6 (PM6) semiempirical methods, and for the MM region (IL solvent), classical force fields (FF) were employed, with the FF developed within the group. The calculated activation free energy barriers (ΔG^\ddagger) for the S_N2 reaction in the presence of $[C_4mim][OMs]$ and $[C_4mim][BF_4]$ ILs were in agreement with the experimental values reported in the literature. On the other hand, only predicted values were obtained for the activation energies for the $[C_4mim][CF_3COO]$, $[C_4mim][Br]$, and $[C_4mim][Cl]$ ILs. These activation energies indicated that the S_N2 reaction would be more facile to proceed using the $[C_4mim][Cl]$ and $[C_4mim][OMs]$ ILs, in contrast with the use of $[C_4mim][Br]$ IL, which presented the highest activation energy. Energy-pair distributions, radial distribution functions, and noncovalent interactions (NCI) were also calculated to elucidate the molecular interactions between the reactive QM region and the solvents or reaction media. From these calculations, it was found that not only the reactivity can be enhanced by selecting a specific anion to increase the K–F separation but also the cation plays a relevant role, producing a synergetic effect by forming hydrogen bonds with the fluorine atom from KF and with the oxygen atoms within the mesylate leaving group. Three interactions are significant for the IL catalytic behavior, $F_{QM}-HX$, $K_{QM}-anion$, and $O_{QM}-HX$ interactions, where the F_{QM} and K_{QM} labels correspond to fluorine and potassium atoms from the KF salt, O_{QM} corresponds to oxygen atoms within the mesylate leaving group (reactant), and HX refers to hydrogen atoms within the IL cation. The NCI analysis revealed that $K_{QM}-anion$ interactions are of weak type, indicating the importance of hydrogen bond interactions from the cation such as $F_{QM}-HX$ and $O_{QM}-HX$ for the catalytic behavior of ILs.



INTRODUCTION

Ionic liquids (ILs) are chemical compounds composed of oppositely charged ions, i.e., cations and anions; however, unlike common molten or fused salts, ILs are liquids at temperatures below 100 °C.^{1,2} This liquid state is favored from the bulky asymmetry of its ions, making their packing difficult.^{1,3,4} Selecting or modifying the nature of the cation in the IL has an effect on its viscosity,^{5,6} melting point,^{7,8} performance as a reaction medium,⁹ and gas solubility in a small degree,^{6,10} whereas the modification of the anion in IL has a large effect on gas solubility,^{10,11} decomposition

temperature,⁷ and catalytic capacity.¹² By combining different cations and anions, it is possible to produce ILs with different properties such as low vapor pressure,^{13,14} a wide range of thermal stabilities,^{7,15,16} densities,^{7,12} gas solubilities,^{10,12}

Received: April 9, 2020

Published: April 30, 2020



Electronic Circular Dichroism of Fullerenols

J. Cornejo-Jacob, J. Vicente-Santiago, and R. A. Guirado-López*

Cite This: *J. Phys. Chem. C* 2020, 124, 7458–7466

Read Online

ACCESS |



Metrics & More

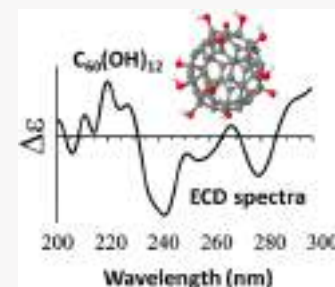


Article Recommendations



Supporting Information

ABSTRACT: We present extensive time-dependent density functional theory calculations dedicated to analyzing the optical properties of model low-hydroxylated $C_{60}(OH)_{12}$ fullerenols. In all our considered isomers, the simulated UV–vis spectra show similar features having in general two well-defined absorption maxima approximately located at 220 and 300 nm. In addition, we calculate, for the first time, the electronic circular dichroism (ECD) spectra of $C_{60}(OH)_{12}$ fullerenols. We obtain that the adsorption of OH groups on the C_{60} surface can reduce the symmetry of the molecular complex, resulting in the appearance of notable optical activity in these kinds of carbon nanostructures made of achiral components. The here-predicted ECD spectra strongly depend on the structure of the OH overlayer, extends from the ultraviolet to the infrared regions, and shows precise features than can be used to distinguish the presence of specific $C_{60}(OH)_{12}$ isomers in a sample. We conclude that in the case of low hydroxylated fullerenols, chirality can be induced by modifying the adsorbed configuration of the OH groups, providing thus novel biological applications for these carbon compounds. We hope our results could motivate optical activity experiments on these kinds of systems.



1. INTRODUCTION

In the last years, it has been clearly established that the properties of C_{60} fullerenes can be strongly altered by the chemical functionalization of its surface.^{1–5} This type of organic derivatives has been found to play an important role in material science,^{6–8} as well as for realizing biomedical^{9–12} and catalytic^{13–15} applications where the solubility and the charge density distribution are key variables to achieve their optimal functionality. In particular, hydroxylated fullerenes^{9–12,15,16} have been the subject of intense research in the last decade since they can be synthesized by various (and relatively easy) experimental techniques. Clearly, different fabrication procedures can lead to the formation of C_{60} cages covered with OH groups adopting various adsorbed phases, which are currently unknown. This is important to emphasize since the properties of $C_{60}(OH)_x$ fullerenols are expected to strongly depend on the amount and distribution of the hydroxyl species. In this respect, extensive experimental characterization has been performed employing Fourier transform infrared spectroscopy (FTIR),¹⁷ transmission electron microscopy (TEM),^{9–11} dynamic light scattering (DLS),¹⁸ and X-ray photoelectron spectroscopy (XPS)^{17,19} in condensed, liquid, and gas phases, and important aspects related to their structure, chemical composition, and aggregation behavior have been revealed.

However, despite the intense research activity mentioned above, it is important to emphasize that none of the previous experimental methods can provide us with the absolute atomic configuration of these complex (sub-nanometer sized) fullerene systems, information that is of fundamental importance to understand the observed macroscopic behavior. Consequently, it is necessary to consider the use of additional spectroscopic techniques that can allow us to obtain structural

information that goes beyond the actual experimental evidence. In this respect, optical spectroscopy could play a fundamental role since the optical response of a molecule and its molecular (and electronic) structure are strongly correlated. Here, it is important to emphasize that even if measurements of the UV–vis spectra of different fullerene complexes typically look very similar, this is not the case for the electronic circular dichroism (ECD) spectra of the samples.^{20–23} As is well known, the ECD detects small differences in the UV–vis spectra between right and left circularly polarized light, is more detailed and structured, and is more sensitive to the composition and local atomic environment of the molecules. Actually, fullerene complexes with very similar structure can produce contrasting spectral patterns in the CD signals, providing thus a possibility for their identification by analyzing the sign and intensity of the Cotton effect at a specific nanometer range.^{24–27}

The possible appearance of the optical activity in fullerenols is relevant to analyze since some of its molecular properties are expected to be altered by chirality. This is particularly important in the field of biology (where chiral molecules are highly abundant in living creatures) since several studies have shown interesting activity in photodynamic therapy^{28–30} and neuroprotection^{31,32} for these compounds. Furthermore, chiral recognition applications as well as the development of highly

Received: December 19, 2019

Revised: March 9, 2020

Published: March 12, 2020



Risk assessment methodology for trajectory planning in keyhole neurosurgery using genetic algorithms

Iván Villanueva-Naquid¹ | Carlos Soubervielle-Montalvo¹ | Ruth M. Aguilar-Ponce² | Saúl Tovar-Arriaga³ | Juan C. Cuevas-Tello¹ | Cesar A. Puente-Montejano¹ | Marcela Mejia-Carlos⁴ | Jaime G. Torres-Corzo⁵

¹Engineering Faculty, Autonomous University of San Luis Potosí, San Luis Potosí, México

²Sciences Faculty, Autonomous University of San Luis Potosí, San Luis Potosí, México

³Engineering Faculty, Autonomous University of Querétaro, Querétaro, México

⁴Optical Communication Research Institute, Autonomous University of San Luis Potosí, San Luis Potosí, México

⁵Department of Neurosurgery, Hospital Central Dr. Ignacio Morones Prieto, San Luis Potosí, México

Correspondence

Iván Villanueva-Naquid, Engineering Faculty, Autonomous University of San Luis Potosí, San Luis Potosí 78090, México.
Email: ivannaquid@gmail.com

Abstract

Background: Preoperative assessment to find the safest trajectory in keyhole neurosurgery can reduce post operative complications.

Methods: We introduced a novel preoperative risk assessment semiautomated methodology based on the sum of N maximum risk values using a generic genetic algorithm for the safest trajectory search.

Results: A set of candidate trajectories were found for two surgical procedures. The trajectories search is done using a risk map considering the proximity of voxels within risk structures in multiple points and a genetic algorithm to avoid an exhaustive search. The trajectories were validated by a group of neurosurgeons.

Conclusions: The trajectories obtained with the proposal method were shorter in 5% and have greater distance from the voxels within the blood vessels in 4.7%. The use of genetic algorithm (GA) speeds up the search for the safest trajectory, decreasing in 99.9% the time required for an exhaustive search.

KEYWORDS

genetic algorithms, keyhole neurosurgery, risk assessment, robotic surgery, trajectory planning

1 | INTRODUCTION

One of the main concerns of neurosurgeons in performing brain surgical interventions is to minimize the damage caused during a surgical procedure. The goal of minimally invasive surgery is to operate with a minimum of trauma while achieving maximal surgical efficiency.¹ Therefore, planning surgical trajectories is of vital importance for neurosurgeons. For minimally invasive exposure, the craniotomy should be as small as possible but as large as necessary for achieving maximal surgical effect, avoiding surgery-related complications.²

Keyhole neurosurgery is an invasive intervention that attempts to reach a target area in the brain. The main goal is to find the best corridor to make a straight trajectory that is easier to perform. A poor decision in the trajectory selection could lead to cause further complications such as bleeding, damage of fundamental cerebral functions, or even death.³ In order to achieve a considerable risk reduction in surgical

interventions, the search for incision areas and trajectories with lower risk is a great topic of interest for neurosurgeons. The problem of planning surgical trajectories can be divided into two stages: assessment of risk values for each considered voxel and search of the minimum risk trajectory.

Modern medical imaging techniques have given rise to the development of methodologies for the construction of data analysis systems for medical applications such as lesion segmentation and diseases diagnosis.⁴⁻⁶ Such systems use information extracted from medical images data sets obtained by computed tomography (CT) or magnetic resonance imaging (MRI), providing surgeons with tools for better decision making.

Robotic-assisted surgery techniques have been used in skull base surgery,⁷ biopsy of intracranial lesions,⁸ deep brain stimulation (DBS),^{9,10} among others. It may be that in the future autonomous robotic neurosurgery will achieve a high level of accuracy and safety



OPEN

Temperature-dependent infrared ellipsometry of Mo-doped VO₂ thin films across the insulator to metal transition

S. Amador-Alvarado¹, J. M. Flores-Camacho¹, A. Solís-Zamudio¹, R. Castro-García², J. S. Pérez-Huerta³, E. Antúnez-Cerón^{5,6}, J. Ortega-Gallegos¹, J. Madrigal-Melchor³, V. Agarwal⁴ & D. Ariza-Flores²✉

We present a spectroscopic ellipsometry study of Mo-doped VO₂ thin films deposited on silicon substrates for the mid-infrared range. The dielectric functions and conductivity were extracted from analytical fittings of Ψ and Δ ellipsometric angles showing a strong dependence on the dopant concentration and the temperature. Insulator-to-metal transition (IMT) temperature is found to decrease linearly with increasing doping level. A correction to the classical Drude model (termed Drude-Smith) has been shown to provide excellent fits to the experimental measurements of dielectric constants of doped/undoped films and the extracted parameters offer an adequate explanation for the IMT based on the carriers backscattering across the percolation transition. The smoother IMT observed in the hysteresis loops as the doping concentration is increased, is explained by charge density accumulation, which we quantify through the integral of optical conductivity. In addition, we describe the physics behind a localized Fano resonance that has not yet been demonstrated and explained in the literature for doped/undoped VO₂ films.

Vanadium dioxide (VO₂) undergoes a first-order insulator-to-metal transition (IMT) at a critical temperature (T_c) around 68 °C^{1,2}, which is accompanied by a structural transformation of a low-temperature monoclinic (M, insulator) to high-temperature tetragonal rutile (R, metal) phase. This transition is fully reversible and is a result of an interplay between Mott and Peierls mechanisms^{3,4}, whereas the relative contributions are still a subject of debate⁵. The monoclinic to rutile or intermediate monoclinic phase transitions coincide with large changes in the optical⁶, electrical⁷, thermal⁸, and magnetic properties⁹, making VO₂ one of the most intensively studied phase change materials due to its unique temperature-dependent physicochemical properties and, at the same time, opens exciting new opportunities for the development of novel functional materials with a wide range of technological and industrial applications such as radiative thermal memristors¹⁰, ultrafast tunable nanoplasmonics^{11,12}, uncooled bolometers¹³, energy-efficient smart windows^{14–17}, heat storage devices¹⁸, temperature sensors¹⁹, ultrafast tunable opto-electronic nano-gating²⁰, room temperature hydrogen nanosensors²¹, infrared optical limiters²², memory and neuromorphic devices⁴, and tunable terahertz metamaterials²³, among others.

Some of the above applications critically rely on the performance of the VO₂ IMT close to ambient conditions. To enhance the application of VO₂ in thermally-triggered optical and electrical switching devices, for instance, the shifting and effective control of its phase transition temperature to around room temperature is highly

¹Instituto de Investigación en Comunicación Óptica, Universidad Autónoma de San Luis Potosí, Alvaro Obregón 64, San Luis Potosí, S.L.P., 78000, Mexico. ²CONACYT-UASLP, Instituto de Investigación en Comunicación Óptica, Universidad Autónoma de San Luis Potosí, Alvaro Obregón 64, San Luis Potosí, S.L.P., 78000, Mexico. ³Unidad Académica de Ciencia y Tecnología de la Luz y la Materia, Universidad Autónoma de Zacatecas, Carretera Zacatecas-Guadalajara km. 6, ejido la Escondida Campus UAZ Siglo XXI edificio E8, Zacatecas, Zac., 98160, Mexico. ⁴Centro de Investigación en Ingeniería y Ciencias Aplicadas, Universidad Autónoma del Estado de Morelos, Av. Universidad 1001 Col. Chamilpa, Cuernavaca, Morelos, 62210, Mexico. ⁵Drug Delivery, Disposition & Dynamics, Monash Institute of Pharmaceutical Sciences, Monash University, Parkville, VIC, 3052, Australia. ⁶Melbourne Centre for Nanofabrication, Victorian Node of the Australian National Fabrication Facility, Clayton, VIC, 3168, Australia. ✉e-mail: david.ariza@cactus.iico.uaslp.mx

Which is better? Experimental and simulation analyses of the chemical modification of carbon nanotubes to improve their dispersion in water

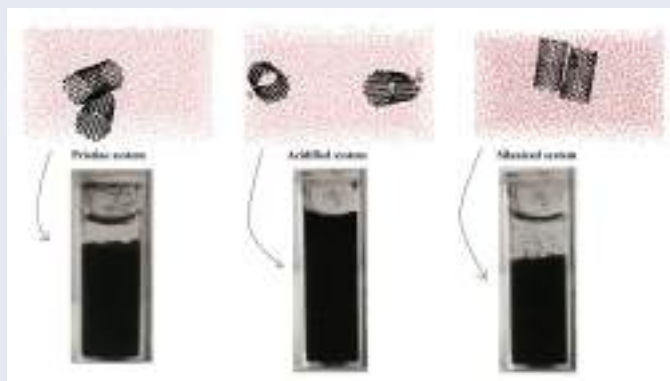
I. Montes-Zavala^a, E. O. Castrejón-González^a, V. Rico-Ramírez^a, Elias Pérez^b, Diego A. Santamaría-Razo^c, and J. A. González-Calderón^d

^aDepartamento de Ingeniería Química, Tecnológico Nacional de México en Celaya, Celaya, Guanajuato, México; ^bInstituto de Física, Universidad Autónoma de San Luis Potosí, San Luis Potosí, México; ^cInnovation Centre for Sustainable Construction, CRH Nederland B.V, Amsterdam, The Netherlands; ^dCátedras CONACYT-Instituto de Física, Universidad Autónoma de San Luis Potosí, San Luis Potosí, México

ABSTRACT

This work combines molecular dynamics with experimental results to explain the behavior of the two main functionalization alternatives of carbon nanotubes (acidification and silanization) when they are dispersed in water. It was observed that the presence of carboxyl and hydroxyl groups in the carbon nanotubes improves the interaction with the aqueous medium by 22% in comparison with the pristine and silanized material. This indicates that the process of acidifying carbon nanotubes to improve their dispersion in aqueous systems is preferable and it is not necessary to employ an additional silanization stage. Experimental studies show that the silanization process induces partial stability because of the positive charges on the surface material, whereas the acidified system is stable for up to 24 hours. On the one hand, pristine and silanized nanotubes show the formation and rupture of the agglomerates; on the other hand, the acidified system shows a behavior similar from that of water, since appropriate interactions occur between the nanotubes and the water molecules. Computational studies were used to evaluate the performance of the systems by calculating the diffusion coefficient and the potential energy of the system. The energy of the system relates to intermolecular interactions between the species involved; greater intermolecular forces guarantee a better integration of the nanotubes, since the forces do not represent an impediment either for the medium to flow or for the nanomaterial to diffuse within the medium. In addition, the distribution of the charge on the surface of the carbon nanotubes guarantees repulsion between them, improving colloidal stability.

GRAPHICAL ABSTRACT



ARTICLE HISTORY

Received 2 December 2019
Accepted 26 April 2020

KEYWORDS

MWCNT colloidal stability;
chemical functionalization;
molecular dynamics;
diffusion coefficient

1. Introduction

Solid carbon structures with sp^2 bond can form a variety of graphitic structures; carbon nanotubes (CNT), discovered in 1991 by S. Iijima,^[1] represent the most interesting and useful of them. Recent studies have reported the synthesis of lignin based carbon nanotubes, which provide bio-based

alternatives to substitute fossil-based high-performance materials.^[2] Carbon nanotubes have several applications. They can improve elastic performance when incorporated into composites, perhaps due to the isotropic orientation of nanotubes within the polymer matrix;^[3] even low percentages of carbon nanotubes have significant effects on the

Hidden attractors from the switching linear systems

F. Delgado-Aranda^{a,*}, I. Campos-Cantón^a, E. Tristán-Hernández^a, and P. Salas-Castro^b

^a*Instituto de Investigación en Comunicación Óptica, Universidad Autónoma de San Luis Potosí,
Alvaro Obregón 64, 78000 San Luis Potosí, S.L.P., México,*

**e-mail: fdelgadoaranda@gmail.com*

^b*Universidad Politécnica de San Luis Potosí,
Urbano Villalón 500, 78363 San Luis Potosí, S.L.P., México.*

Received 14 January 2020; accepted 21 May 2020

Recently, chaotic behavior has been studied in dynamical systems that generate hidden attractors. Most of these systems have quadratic nonlinearities. This paper introduces a new methodology to develop a family of three-dimensional hidden attractors from the switching of linear systems. This methodology allows to obtain strange attractors with only one stable equilibrium, attractors with an infinite number of equilibria or attractors without equilibrium. The main matrix and the augmented matrix of every linear system are considered in Rouché-Frobenius theorem to analyze the equilibrium of the switching systems. Also, a systematic search assisted by a computer is used to find the chaotic behavior. The basic chaotic properties of the attractors are verified by the Lyapunov exponents.

Keywords: Chaos; hidden attractor; equilibrium; linear system

PACS: 02.10.Ud; 02.10.Yn; 05.45.Pq; 82.40.Bj

DOI: <https://doi.org/10.31349/RevMexFis.66.683>

1. Introduction

The first chaotic system was introduced by Edward Lorenz [1]. From this, the interest in developing new similar systems emerged, and it has been applied in several applications such as securing communications [2], synchronization of systems [3], power systems [4], among others. In dynamical systems, equilibrium is an important characteristic, since the motion of trajectories depend on the local behavior around the neighborhood of the fixed point. Most of the chaotic systems reported in the literature have a determined number of equilibria, and these have been widely studied. For instance, the Lorenz [1], Chen [5], Lü [6] and Chua [7] systems have three equilibrium points, and the Rössler system [8] has only two equilibrium points. Likewise, Sprott [9] has proposed a set of chaotic systems where some of them have only one or two equilibrium points. Moreover, some chaotic systems have an equilibrium point in each basin of attraction which is generated by a piecewise linear function (PWL) [10–12]. The PWL function allows to obtain a set of linear systems, each one having a hyperbolic equilibrium point. These systems can generate three or more scrolls in an attractor; thus, they are known as *multi scroll attractors*.

Similar systems have been studied with two or more positive Lyapunov exponents. According to [13], these dynamical systems are called *hyperchaotic*.

In recent years, some systems that generate chaotic attractors which their basin of attraction does not intersect with its neighborhoods of the equilibrium points have been found, these are known as hidden attractors. Hidden attractors are difficult to find because both basins of attraction and the dimension of the attractor could be very small. According to [14], the systems with hidden attractors are classified as a hidden attractor without equilibrium, a hidden attractor with an infinite number of equilibria, and a hidden attractor with

one stable equilibrium. For these systems, it is not possible to apply the Shilnikov theorem [15, 16] to demonstrate the existence of chaos, because they do not have homoclinic and heteroclinic orbits.

From Sprott's A-system [9], chaotic systems without equilibrium such as Pham [17], C. Wang [18], Azar [19], Wei [20] and Jafari [21] systems have been developed. Also, hyperchaotic systems [22], multi scroll systems [23–25], and fractional-order systems [26, 27] without equilibrium have been studied.

On the other hand, some authors have developed chaotic systems that present an infinite number of equilibria. For instance, Jafari [28], Chumbiao [29] and Li [30] systems. Besides it has been found that some hyperchaotic systems [31] and fractal-order systems [32] has a line of equilibria.

Finally, the systems with only one stable equilibrium have been studied from the Sprott's E-system. Some authors, such as Wang [33], Pham [34], among others, proposed similar systems through quadratic nonlinearities. Also, systems with two stable equilibria [35, 36] have been developed, and this opens the possibility to design multi scroll systems in the future.

Notice that the chaotic systems mentioned above present quadratic nonlinearities. However, there are a few systems in the literature that generate hidden attractors from switching linear systems [37, 38]. In these researches, the main methodology is to find hidden degeneracies in piecewise smooth dynamical systems through the sliding mode methods, and they use of efficient analytical-numerical methods for the study of hidden attractors. The approach is based on the use of modern computers and the development of numerical methods. Chua's system was used to find hidden attractors through these approaches. Due to this motivation, this work presents a new methodology to develop a family of three-dimensional



Overlapping effects of the optical transitions of GaNAs thin films grown by molecular beam epitaxy

I.E. Cortes-Mestizo^{a,*}, L.I. Espinosa-Vega^b, J.A. Espinoza-Figueroa^b, C.M. Yee-Rendón^c,
L. Zamora-Peredo^d, A.G. Rodríguez^b, C.A. Mercado-Ornelas^b, F.E. Perea-Parrales^b,
V.H. Méndez-García^b

^a CONACYT- Coordinación para la Innovación y la Aplicación de la Ciencia y la Tecnología (CIACYT), Universidad Autónoma de San Luis Potosí, Av. Sierra Leona #550, Col. Lomas 2a Sección, San Luis Potosí, San Luis Potosí, 78210, México

^b Coordinación para la Innovación y la Aplicación de la Ciencia y la Tecnología (CIACYT), Universidad Autónoma de San Luis Potosí, Av. Sierra Leona #550, Col. Lomas 2a Sección, San Luis Potosí, San Luis Potosí, 78210, México

^c Facultad de Ciencias Físico-Matemáticas, Universidad Autónoma de Sinaloa, Av. de las Americas y Blvd. Universitarios, Culiacán, Sinaloa, 80000, México

^d Centro de Investigación en Micro y Nanotecnología, Universidad Veracruzana, Calzada Ruiz Cortines #455, Boca del río, Veracruz, 94294, México

ARTICLE INFO

Keywords:

Gallium arsenide nitride
Conduction band splitting
Photoreflectance
Ellipsometry
Molecular beam epitaxy
GaNAs/GaAs heterojunction
Band anti-crossing model
Dilute nitride

ABSTRACT

Photoreflectance and ellipsometry are two very useful optical spectroscopy techniques employed to analyze the electronic band structure of semiconductors. Photoreflectance and ellipsometry spectra of gallium arsenide nitride (GaNAs) thin films on gallium arsenide (GaAs) layers may be composed of transitions from the conduction bands of the alloy and the binary (E_c , E_{c+} , and E_{c0} , respectively) in conjunction with their interaction spin-orbit split-off valence band ($E_v + \Delta_0$ and $E_{v0} + \Delta_0$). For low concentration of nitrogen (between 0.2 and 0.6 %), the determination of the E_{c+} conduction band becomes difficult to distinguish by the fact that critical points are superimposed in the spectrum of both characterization techniques. In this work, a method to determine the E_{c+} conduction band of GaNAs thin films grown on GaAs by molecular beam epitaxy is proposed when the overlapping of spectral features influences their optical determination. When using spectroscopic characterization techniques, the modulation/excitation region depends on the wavelength employed and sample characteristics, and consequently low nitrogen concentration in the alloy in conjunction with the thickness of the GaNAs layers have been found responsible for the signal overlapping. It is demonstrated that by decreasing the sample temperature in the photoreflectance process the overlapping is avoided, allowing for a correct interpretation of the GaNAs conduction band splitting analysis and discarding the contribution of built-in electric fields. From these results, we achieved a precise experimental determination of the presence/absence of the band splitting predicted by the band anti-crossing model using non-destructive characterization tools.

1. Introduction

Through the substitution of arsenic by nitrogen atoms in the gallium arsenide (GaAs) host lattice the gallium arsenide nitride ($\text{GaN}_x\text{As}_{1-x}$, where x is the mole fraction of N) ternary compound is formed. This material has been widely researched due to the attractive large bandgap bowing observed even for small atomic percentage of nitrogen (%N) incorporation since it was experimentally demonstrated in the early 1990s [1]. For instance, within the diluted regime (%N < 3) the band gap energy is reduced by ~ 100 meV per %N [2]. On this way, the development of the GaNAs has been a subject of great interest due to the potential applications in optoelectronic devices, covering emission/

absorption processes between red to ultraviolet [3-6].

The behavior of the band structure of the GaNAs system is explained by the band anti-crossing model (BAC), which describes the role of nitrogen incorporation on a wide variety of III-N-V alloys. The BAC indicates that anti-crossing interaction between the electronic states of the localized nitrogen and energy states of the GaAs host matrix split the conduction band into two sub-bands labeled as E_c and E_{c+} [7]. The band gap of the GaNAs system is related to E_c while the E_{c+} level is an extra conduction-band edge of the GaNAs. Thus, the $\text{GaN}_x\text{As}_{1-x}$ bandgap can be tuned in by the %N used in the alloy, according to BAC. As it was mentioned earlier, a small increment of %N decreases the bandgap energy, E_c , while at the same time increases the energy separation

* Corresponding author.

E-mail address: irving.cortes@uaslp.mx (I.E. Cortes-Mestizo).

<https://doi.org/10.1016/j.tsf.2020.137969>




Received 12 September 2019; Received in revised form 7 February 2020; Accepted 18 March 2020

Available online 20 March 2020

0040-6090/ © 2020 Elsevier B.V. All rights reserved.

Article

Structure, Acidity, and Redox Aspects of VO_x/ZrO₂/SiO₂ Catalysts for the n-Butane Oxidative Dehydrogenation

José-Luis Sánchez-García ¹, Brent E. Handy ¹, Ilse N. Ávila-Hernández ¹,
Angel G. Rodríguez ², Ricardo García-Alamilla ³ and Maria-Guadalupe Cardenas-Galindo ^{1,*}

¹ Facultad de Ciencias Químicas, Universidad Autónoma de San Luis Potosí (UASLP), Av. Manuel Nava #6, San Luis Potosí, S.L.P. 78210, Mexico; luis.sanchez@uaslp.mx (J.-L.S.-G.); handy@uaslp.mx (B.E.H.); ilse3571@hotmail.com (I.N.Á.-H.)

² Coordinación para la Innovación y la Aplicación de la Ciencia y la Tecnología, UASLP, Álvaro Obregón 64, San Luis Potosí, S.L.P. 78000, Mexico; angel.rodriguez@uaslp.mx

³ Centro de Investigación en Petroquímica, Tecnológico Nacional de México, Instituto Tecnológico de Ciudad Madero, Altamira, Tamps 89600, Mexico; ricardogarcia.alamilla@yahoo.com.mx

* Correspondence: cardenas@uaslp.mx; Tel.: +52-444-826-2440 (ext. 6468)

Received: 1 April 2020; Accepted: 5 May 2020; Published: 15 May 2020



Abstract: ZrO_x/SiO₂ and VO_x/ZrO_x/SiO₂ catalysts (5 wt %–25 wt % Zr, 4 wt % V) were prepared by grafting zirconium and vanadium alkoxides on Aerosil 380. All samples were characterized by temperature programmed reduction, N₂ physisorption, X-ray diffraction, Raman spectroscopy, and ammonia adsorption microcalorimetry. Tetragonal ZrO₂ and zircon (ZrSiO₄) were present at 25 wt % Zr, but only amorphous zirconia overlayer existed for lower loadings. At lower Zr loadings (5 wt %–10 wt % Zr), exposed silica surface leads to V₂O₅ crystallites and isolated VO₄ species, although V reducibility behavior changes, from being similar to VO_x/SiO₂ (5 wt % Zr) to showing VO_x/ZrO₂ behavior at 10 wt % Zr, and a diminished total amount of reducible V. Highly acidic ZrO₂ sites are covered by the vanadium grafting, forming weaker sites (60–100 kJ/mol NH₃ adsorption strength). Catalytic conversion and selectivity for the oxidative dehydrogenation of n-butane (673 K, n-C₄/O₂ = 2.2) over VO_x/ZrO_x/SiO₂ show that 1,3-butadiene is favored over cis-2-butene and trans-2-butene, although there is some selectivity to the 2-butenes when VO_x/ZrO₂ behavior is evident. At low Zr loadings, butadiene formed during reaction acts as the diene species in a Diels–Alder reaction and gives rise to a cyclic compound that undergoes further dehydrogenation to produce benzaldehyde.

Keywords: V₂O₅/ZrO₂; butane ODH; adsorption microcalorimetry; TPR; Raman; Diels–Alder

1. Introduction

The last few years have seen a growing interest in cycloaddition reactions, such as Diels–Alder, followed by dehydrogenation to produce aromatic compounds in a novel fashion from diverse feedstocks, such as those that come from biomasses [1]. An important aromatic compound used in the food, perfume, and pharmaceutical industry is benzaldehyde, with the requirement that it must be free of toxic impurities. Currently, commercial benzaldehyde production occurs by either toluene oxidation or the hydrolysis of benzal chloride. However, both processes cannot be considered as green technologies, as the benzaldehyde produced may contain benzoic acid or chlorine residues [2] that must be removed, which complicates the design of the separation process system. In the past decade, interest has been focused on the heterogeneous oxidation of benzyl alcohol to benzaldehyde [3–9],

Use of Chemically Modified Titanium Dioxide Particles to Mediate the Non-isothermal Cold Crystallization of Poly(lactic acid)

Guadalupe Mendoza^{1†}, M.G. Peña-Juárez^{2†}, J.A. Gonzalez-Calderon^{3,*}, Elías Pérez^{4,*}

¹Doctorado en Ciencias Ingeniería Química. Universidad Autónoma de San Luis Potosí, Av. Manuel Nava #6, Zona Universitaria, 78290 San Luis Potosí, San Luis Potosí, México.

²Doctorado Institucional en Ingeniería y Ciencia de Materiales. Universidad Autónoma de San Luis Potosí, Sierra Leona No. 550 Col. Lomas 2da. Sección, 78210 San Luis Potosí, San Luis Potosí, México.

³Cátedras CONACYT-Instituto de Física, Universidad Autónoma de San Luis Potosí, Álvaro Obregón #64, 78000, San Luis Potosí, San Luis Potosí, México.

⁴Instituto de Física, Universidad Autónoma de San Luis Potosí, Álvaro Obregón #64, 78000 San Luis Potosí, San Luis Potosí, México.

†* Equally contribution.

*Corresponding author: J. A. Gonzalez-Calderon, email: amir@ifisica.uaslp.mx, Elías Pérez, email: elias@ifisica.uaslp.mx

Received December 1st, 2019; Accepted February 8th, 2020.

DOI: <http://dx.doi.org/10.29356/jmcs.v64i2.1126>

Abstract. In this work, the effect of the chemical modification of titanium dioxide particles on the non-isothermal crystallization process of polylactic acid (PLA) was studied. Cold crystallization in some polymers occurs above the glass transition temperature (T_g) when the polymer chains gain sufficient mobility to organize themselves into the ordered structure (i.e. the crystal structure) by folding the chains. Cold crystallization in general is caused by the ordering of the molecular chains in the crystalline PLA due to the increased mobility during heating. Through an analysis of the cool crystallization process in DSC at different cooling rates, it was observed that the behavior of PLA and its composites made with titanium dioxide, neat and functionalized with dicarboxylic acids, can be described through the models used for crystallization of the polymer carrying out during cooling, such as Mo's and Jeziorny's model. In addition, it was determined that the chemical modification of TiO_2 performed with silane increases the crystallization rate in the last step of the process; while the chemical modification with dicarboxylic acid has an accelerated effect on the crystal formation process attributed to the affinity between the aliphatic part of this group and the polymer chains. Also, it was shown that the inclusion of the silanized particles has no effect on the energy requirement compared to the pure PLA process; however, the addition of particles with the dicarboxylic acid decreases the energy value required to complete the crystalline state due to affinity at the surface to immobilize the polymer chains. Finally, it is emphasized that the activation energy required to perform the crystallization of PLA and its composites has positive values, which is an indicator that the crystallization was performed while heating, after reaching and passing the glass transition temperature and before melting.

Keywords: Non-isothermal crystallization; titanium dioxide; composites; chemical modification; poly(lactic acid).

Resumen. En este trabajo, se estudió el efecto de la modificación química de partículas de dióxido de titanio en el proceso de cristalización no isotérmica del ácido poliláctico (PLA). La cristalización en frío en algunos polímeros ocurre por encima de la temperatura de transición vítrea (T_g) cuando las cadenas de polímero ganan suficiente movilidad para organizarse en la estructura ordenada (es decir, la estructura cristalina) al doblar las



Real-time reflectance anisotropy spectroscopy of GaAs homoepitaxy

A. LASTRAS-MARTÍNEZ,^{1,*} L. E. GUEVARA-MACÍAS,¹ J. G. SANTIAGO-GARCÍA,¹
J. ORTEGA-GALLEGOS,¹ I. A. RUIZ-ALVARADO,¹ R. MARTÍNEZ-ESPINOSA,¹ D. ARIZA-FLORES,²
R. CASTRO-GARCÍA,² R. E. LÓPEZ-ESTOPIER,² R. E. BALDERAS-NAVARRO,¹
AND L. F. LASTRAS-MARTÍNEZ¹

¹Instituto de Investigación en Comunicación Óptica, Universidad Autónoma de San Luis Potosí, San Luis Potosí, S.L.P. 7800 México, Mexico

²CONACyT - Universidad Autónoma de San Luis Potosí, Instituto de Investigación en Comunicación Óptica, San Luis Potosí, S. L. P. 78000 México, Mexico

*Corresponding author: alm@cactus.iico.uaslp.mx

Received 19 November 2019; revised 7 January 2020; accepted 8 January 2020; posted 10 January 2020 (Doc. ID 383611); published 21 February 2020

Reflectance anisotropy spectroscopy (RAS) is a highly sensitive optical probe for the real-time study of the epitaxial growth of zincblende semiconductors. Here we report on (1) non-equilibrium RAS spectra acquired in real time during the homoepitaxial growth of GaAs, and (2) RAS spectra for GaAs surfaces under equilibrium with several arsenic overpressures. We show that in both cases RAS spectra can be decomposed into two basic components, each with a characteristic line shape. We further show that both dynamic and equilibrium RAS spectra are described by the same pair of basic components. We conclude that the time evolution of non-equilibrium RAS spectra acquired during the epitaxial growth can be described in terms of RAS spectra for equilibrium surfaces. The results reported here should be useful for the interpretation of the physics underlying the rapid time evolution of dynamic RAS spectra during the first monolayer growth. Thus, we show that RAS constitutes a valuable tool for the study of epitaxial growth mechanisms. © 2020 Optical Society of America

<https://doi.org/10.1364/AO.383611>

1. INTRODUCTION

The growing complexity of advanced optoelectronic devices based on III-V semiconductors demands probes for real-time growth monitoring with sub monolayer (ML) resolution. Non-invasive optical probes such as reflectance anisotropy spectroscopy (RAS) are advantageous for this application given their high sensitivity, instrumental simplicity, and fast response. RAS is an optical polarization contrast technique, based on the measurement of the difference of reflectivity for two orthogonal polarized light beams. This spectroscopy enhances the surface related response by taking advantage of the reduced symmetry of the surface region of a cubic crystal [1,2]. In this respect, we note that for polarizations of the incident beam parallel to the principal axes of the crystal, the signal arising from the isotropic bulk is suppressed [3].

For the molecular beam epitaxy (MBE) homoepitaxial growth of GaAs (001) on As-rich surfaces it is known that the RAS spectra comprise two independent components with well-differentiated line shapes [4]. A first component rises sharply upon starting growth while the second component remains relatively constant. The rapid changing component has been

associated with strains induced by surface reconstructions [4]. By contrast, the physical origin of the second component is not presently understood. To help shed light on the physical origin of the optical anisotropies of the growing surface, in this paper we report on RAS measurements carried out to determine to what extent dynamic RAS spectra of growing surfaces correspond to RAS spectra of surfaces in equilibrium under a fixed As overpressure. We show that both dynamic and equilibrium spectra are consistent with each other so that RAS spectra acquired during epitaxial growth can be understood as a succession of equilibrium spectra.

2. EXPERIMENTAL

The GaAs epitaxial growth was carried out in a Riber 32 MBE growth chamber equipped with a solid-source Ga effusion cell and a valved As-cracker cell at a substrate temperature of 570°C and an As overpressure of $P_{As} = 10^{-6}$ Torr. An optical window placed in front of the substrate in growth position allows for carrying out RAS measurements in real time during epitaxial growth. RAS measurements were carried out with a recently developed rapid RAS spectrometer at an acquisition rate of 10

GaAs/InGaAs heterostructure strain effects on self-assembly of InAs quantum dots

C. A. Mercado-Ornelas^a, I. E. Cortes-Mestizo^b, E. Eugenio-López^{a, g}, L.I. Espinosa-Vega^a, D. García-Compean^b, A.Yu. Gorbachev^c, L. Zamora-Peredo^d, C.M. Yee-Rendon^f and V. H. Méndez-García^{a,*}

^a *Center for the Innovation and Application of Science and technology, Universidad Autónoma de San Luis Potosí (UASLP), Av. Sierra Leona #550, Col. Lomas 2a Sección, 78210, San Luis Potosí, México.*

^b *CONACYT-Center for the Innovation and Application of Science and technology, Universidad Autónoma de San Luis Potosí (UASLP), Av. Sierra Leona #550, Col. Lomas 2a Sección, 78210, San Luis Potosí, México.*

^c *Departamento de Ingeniería Eléctrica, Electrónica y Mecatrónica, Tecnológico Nacional de México-Instituto Tecnológico de San Luis Potosí, México.*

^d *Optical Communications Research Institute, Universidad Autónoma de San Luis Potosí, Av. Karakorum #1470, Lomas 2ª Secc. C.P. 78210, San Luis Potosí, México.*

^e *Centro de Investigación en Micro y Nanotecnología, Boca del Río, Veracruz, México.*

^f *Facultad de Ciencias Físico-Matemáticas, Universidad Autónoma de Sinaloa, Culiacán, Sinaloa, México.*

^g *Zentrum für Oberflächen-und Nanoanalytik Johannes Kepler University, Linz, Austria.*

*Corresponding author: victor.mendez@uaslp.mx

Biosynthesis and characterization of cadmium carbonate crystals by anaerobic granular sludge capable of precipitate cadmium

CM Martínez*, M. Rivera-Hernández, Luis H. Álvarez, Ismael Acosta-Rodríguez, Ruíz F, VD Compeán-García**

M. Rivera-Hernández Facultad de Ciencias, Universidad Autónoma de San Luis Potosí. Lateral Av. Salvador Nava Martínez S/N, Zona Universitaria, San Luis Potosí, SLP México 78290. E.mail: Luna_Marix@hotmail.com

Luis H. Álvarez Departamento de Ciencias Agronómicas y Veterinarias, Instituto Tecnológico de Sonora, 5 de Febrero 818 Sur, Ciudad Obregón, Sonora, México 85000. E-mail: luis.alvarez@itson.edu.mx

Ismael Acosta-Rodríguez Facultas de Ciencias Químicas, Universidad Autónoma de San Luis Potosí. Lateral Av. Salvador Nava Martínez S/N, Zona Universitaria, San Luis Potosí, SLP México. ZP. 78290. E.mail: iacosta@uaslp.mx

Ruíz F. Facultad de Ciencias, Universidad Autónoma de San Luis Potosí. Lateral Av. Salvador Nava Martínez S/N, Zona Universitaria, San Luis Potosí, SLP México 78290. E.mail: facundo@fciencias.uaslp.mx

Corresponding authors: **CM Martínez** Facultad de Ciencias, Universidad Autónoma de San Luis Potosí. Lateral Av. Salvador Nava Martínez S/N, Zona Universitaria, San Luis Potosí, SLP México 78290. E-mail: *claudiam.martinezr@gmail.com. Tel.: +52 (444) 3813330

VD. Compeán-García CONACyT-Coordinación para la Innovación y Aplicación de la Ciencia y la Tecnología. Universidad Autónoma de San Luis Potosí. Sierra Leona #550, Lomas de San Luis, 78210 San Luis Potosí E-mail: **damiancompean@gmail.com

Crystalline Truncated Micropyramids Grown from GaAs Liquid Phase on GaP (001) Substrates

Francisco J. Rocha-Reina,* Edith G. Castillo-Baldivia, Osvaldo Del Pozo-Zamudio, Andrés de Luna-Bugallo, Vyatcheslav A. Michournyi, Edgar A. Cerda-Méndez, Raúl E. Balderas-Navarro, and Andrei Gorbachev


Herein, a report on the growth of crystalline truncated pyramid microstructures by liquid-phase epitaxy of Ga–As liquid phase on GaP (001) substrates under nonequilibrium (NEQ) conditions with different contact times and growth temperatures is provided. The micropyramids (MPs) have rectangular bases which are between 5 and 10 μm long, with the long sides aligned with the [110] direction. Remarkably, the results show that the growth rates of the MP under NEQ are very high compared with those of traditional epitaxial layers grown under near-equilibrium conditions. Spatially resolved microphotoluminescence mappings reveal a spatial dependence of the near-band edge emission in both wavelength and intensity within a single MP. The measured emission-wavelength range corresponds to ternary GaAs_{1-x}P_x alloys, which attests to the diffusion of P atoms from the substrate into the MPs during growth. The content of P atoms in the MPs is confirmed by spatially resolved energy-dispersive X-ray spectroscopy. Both studies show that the concentration of P is higher in the {111} planes than in the rest of the MP. A thermodynamic argument is proposed to support the experimental findings.

1. Introduction

The controlled growth of lattice-mismatched epitaxial layers with built-in strains^[1–5] is fundamental to engineer the electronic band structure of semiconductors for the manufacture of optoelectronic devices such as photodiodes,^[6–8] light emitters,^[9] quantum dots,^[10–12] nanowires,^[13] and highly efficient solar cells.^[14,15] In general, in III–V materials, a large lattice mismatch between two materials exists whenever $(a_{\text{epi}} - a_{\text{s}}) - a_{\text{s}} > 2\%$,^[16,17]

F. J. Rocha-Reina, E. G. Castillo-Baldivia, Dr. O. Del Pozo-Zamudio, Dr. V. A. Michournyi, Dr. E. A. Cerda-Méndez, Dr. R. E. Balderas-Navarro, Dr. A. Gorbachev
 Instituto de Investigación en Comunicación Óptica
 Universidad Autónoma de San Luis Potosí
 Av. Karakorum 1470 Lomas 4a, 78210 San Luis Potosí, SLP, México
 E-mail: francisco_rocha@cactus.iico.uaslp.mx

Dr. A. de Luna-Bugallo
 CONACYT-Cinvestav Unidad Querétaro
 Libramiento Norponiente 2000, Fracc. Real de Juriquilla, 76230 Santiago de Querétaro, México

 The ORCID identification number(s) for the author(s) of this article can be found under <https://doi.org/10.1002/pssa.202000164>.

DOI: 10.1002/pssa.202000164

where a_{epi} and a_{s} are the lattice parameters of the epitaxial layer and the substrate, respectively.^[18]



The growth of highly lattice-mismatched III–V semiconductors epitaxial layers is usually done by molecular beam epitaxy (MBE) under the Stranski–Krastanov mode, resulting in the formation of nanometric structures such as quantum dots. Liquid-phase epitaxy (LPE), in contrast, is considered as a low-cost technology for the growth of uniform epitaxial layers in or close to thermodynamic equilibrium. Nevertheless, the growth by LPE of highly mismatched epitaxial layers under nonequilibrium (NEQ) conditions has also been used to fabricate nanometric structures,^[19–22] particularly quantum dots in the InAs/GaAs,^[11,23–25] InSb/InAs or InSb/GaAs,^[26] and PbSe/GaSb^[27] systems.

In this work, we demonstrate a novel LPE growth mode of GaAs liquid phase (LP) on GaP (001) substrates under strong NEQ conditions. In this growth mode, we observe the formation of micrometric crystalline Ga–As–P truncated pyramid structures and growth rates much higher than those formerly reported. We discuss how the NEQ conditions of the system cause overheating of the LP at the liquid–solid interface, resulting in simultaneous dissolution of the substrate and crystallization in separate areas of its surface. The P atoms from the dissolved regions at the substrate surface incorporate into the GaAs LP, affecting the growth rate and the final concentration in the solid phase. We characterize the micropyramids (MPs) using optical inspection, microphotoluminescence measurements (μPL) and energy-dispersive X-ray spectroscopy (EDXRS). We find that the MPs have very good crystalline quality and a volumetric P concentration gradient. Our results shed light on the complex growth processes under NEQ and may be useful for the fabrication of nonplanar devices using LPE.

2. Results

The GaP (solid)/GaAs (liquid) system is under NEQ conditions during the LPE growth due mainly to two factors. First, the group V elements are different in the liquid and solid phases, and, second, there is a large (3.7%) lattice mismatch between the two

Many-electron redistribution in *n*-doped semiconductor nanostructures under external electric field by using a center-of-mass approach

Reyna Méndez-Camacho,^{1,2,*} Ramón Castañeda-Priego¹ ,¹ and Esteban Cruz-Hernández^{2,†} 

¹*División de Ciencias e Ingenierías, Campus León, Universidad de Guanajuato, Loma del Bosque 103, 37150 León, México*

²*Coordinación para la Innovación y Aplicación de la Ciencia y la Tecnología, Universidad Autónoma de San Luis Potosí, Sierra Leona 550, 78210 San Luis Potosí, México*



(Received 19 April 2020; revised 13 June 2020; accepted 16 June 2020; published 1 July 2020)

The study of an external force triggering the many-electron redistribution in nanostructures is of importance for both theoretical and practical interest in condensed matter physics. Hence, the goal of this contribution is to theoretically investigate the influence of an external electric field (EEF) on the ground and excited states of a system of many-electrons confined in GaAs/AlGaAs nanostructures. To deal with the many-body issue, we employ a Yukawa-like potential in a two-electron framework, while it is proposed to explore the challenging EEF contribution by analyzing its effect on the electronic center-of-mass framework. Thus, while the Yukawa-like potential allows us to model the many-electron interaction in the range from 10^{17} to 10^{23} electrons/cm³, via the adjustment of a simple screening parameter; the center-of-mass approximation also allows us to describe easily the effect of the EEF separately. Internal electronic distributions in nanostructures of various sizes and electronic concentrations are obtained and discussed for EEF of variable magnitude. This alternative approach enables us to decouple the electron-electron and the EEF interactions, which is useful in determining the origin of the observed features. We show that this theoretical framework is well suited to get relevant information in semiconductor nanostructures of practical sizes and realistic doped levels.

DOI: [10.1103/PhysRevB.102.035403](https://doi.org/10.1103/PhysRevB.102.035403)

I. INTRODUCTION

Recent advances in nanofabrication and the technology of semiconductor nanostructures, such as quantum wires (QWRs) or quantum dots (QDs) [1–3], promise a wide spectrum of potential applications. The latter are possible due to the deep modification of the nanostructure physical properties, such as sharp density of states, ballistic electronic transport, or enriched optical properties that are quite different to those of the bulk material [3,4].

In particular, because QWRs possess both transversal quantum confinement and longitudinal ballistic transport, extensive experimental and theoretical studies [5–8] have shown their high potential to be applied in the next generation of optoelectronic and electronic devices [9–12]. In most of the nanostructure-based devices, the activation of such properties involves the application of an external voltage (V_{ext}), which in turn produces an EEF (E_{ext}). It is then crucial to deeply understand its impact on the internal electronic reconfiguration and the related modification on the QWRs and QDs properties.

Due to the issues related to the modeling of large (micrometric) wires and high electronic concentrations (around 10^{17} electrons/cm³), most of the reported works address the study of an EEF on semiconductor nanostructures of small (nanometric) size, containing just one or a few electrons.

So, when addressing QWRs, usually a transverse EEF is applied (along the short, nanometric, QWR cross-section) and single electronic or excitons redistribution, known as the Stark effect, are usually reported [13–19]. For example, for semiconductor QDs an electronic Stark shift (in the opposite direction to the EEF and towards lower energies), changes in the photoluminescence emission and optical absorption have been reported [17,18,20]. However, the most common configuration, when the EEF is applied along the wire remains much less studied mainly because it implies dealing with relatively large sizes and many-body electron-electron (*e-e*) interactions, which is a quite challenging issue.

In recent publications, we proposed the use of a Yukawa-like-interaction to deal with the many-body problem, which allows us to describe the *e-e* interaction in *n*-doped semiconductor nanostructures of typical electronic concentrations and realistic lengths [21,22]. By using this formalism, for example, valuable information about the Wigner molecule formation in QWRs, such as critical electronic-densities or optimal geometries were reported for different semiconductor materials. In the present work, we study the effect of an E_{ext} on the electronic distribution in semiconductor GaAs/AlGaAs nanostructures. To this end, the *e-e* is handled as in Ref. [22] while the E_{ext} is decoupled by applying it to the electronic center-of-mass framework of the entire *e-e* interacting system.

Hereafter, we solve the Schrödinger equation by decoupling the *e-e* relative framework from the center-of-mass one of the total electronic distribution. In the two-electron framework, two nonrelativistic electrons in GaAs wells

*reyna.mendez@uaslp.mx

†esteban.cruz@uaslp.mx

Gaussian concentration bound for potentials satisfying Walters condition with subexponential continuity rates

J-R Chazottes^{1,3} , J Moles^{2,4} and E Ugalde^{2,5} 

¹ Centre de Physique Théorique, CNRS, Institut Polytechnique de Paris, France

² Instituto de Física, Universidad Autónoma de San Luis Potosí, S.L.P., 78290, Mexico

E-mail: chazottes@cpht.polytechnique.fr, molesjdn@ifisica.uaslp.mx and ugalde@ifisica.uaslp.mx

Received 20 February 2019, revised 10 September 2019

Accepted for publication 19 November 2019

Published 30 January 2020



CrossMark

Recommended by Dr Mark F Demers

Abstract

We consider the full shift $T : \Omega \rightarrow \Omega$ where $\Omega = A^{\mathbb{N}}$, A being a finite alphabet. For a class of potentials which contains in particular potentials ϕ with variation decreasing like $O(n^{-\alpha})$ for some $\alpha > 2$, we prove that their corresponding equilibrium state μ_ϕ satisfies a Gaussian concentration bound. Namely, we prove that there exists a constant $C > 0$ such that, for all n and for all separately Lipschitz functions $K(x_0, \dots, x_{n-1})$, the exponential moment of $K(x, \dots, T^{n-1}x) - \int K(y, \dots, T^{n-1}y) d\mu_\phi(y)$ is bounded by $\exp(C \sum_{i=0}^{n-1} \text{Lip}_i(K)^2)$. The crucial point is that C is independent of n and K . We then derive various consequences of this inequality. For instance, we obtain bounds on the fluctuations of the empirical frequency of blocks, the speed of convergence of the empirical measure, and speed of Markov approximation of μ_ϕ . We also derive an almost-sure central limit theorem.

Keywords: concentration inequalities, empirical measure, Kantorovich distance, d-bar distance, relative entropy, Markov approximation

Mathematics Subject Classification numbers: 37D35, 60E15

³JRC benefited from an ECOS Nord project for his stay at San Luis Potosí.

⁴JM benefited from an ECOS Nord project for his stay at Ecole Polytechnique.

⁵EU acknowledges Ecole Polytechnique for financial support (one-month stay).

A novel disposable sensor for measure intra-abdominal pressure

Nuevo sensor desechable para medir la presión intraabdominal

José S. Camacho-Juárez^{1*}, Bersaín Alexander-Reyes¹, Antonio Morante-Lezama¹, Martín Méndez-García¹, Hernán González-Aguilar¹, Ildelfonso Rodríguez-Leyva², Oscar F. Nuñez-Olvera³, Carlos Polanco-González⁴, Luis A. Gorordo-Delso⁴ y Jorge A. Castañón-González^{4,5}

¹Facultad de Ciencias, Universidad Autónoma de San Luis Potosí, San Luis Potosí; ²Facultad de Medicina, Universidad Autónoma de San Luis Potosí, San Luis Potosí; ³Instituto de Investigación en Comunicación Óptica, Universidad Autónoma de San Luis Potosí, San Luis Potosí; ⁴Facultad de Ciencias, Universidad Autónoma de México, Ciudad de México; ⁵Unidad de Cuidados Intensivos, Hospital Juárez de México, Ciudad de México. México

Abstract

Background: Measurement of intra-abdominal pressure (IAP) is realized with the Kron's method. However, this technique has drawbacks like an infusion of water into the bladder of the patient. **Objective:** The prove a new novel disposable sensor in the way to measure the IAP (DSIAP) this one addresses some limitations of the Kron method. **Materials and methods:** The DSIAP was tested in vitro and clinical settings. The proposed technique was compared with Kron's method through Pearson correlation and Bland-Altman analysis. For in vitro tests, 159 measurements were taken performed by simulating the IAP in the bladder. For the clinical test, 20 pairs of measurements were made in patients with routine IAP monitoring in the intensive care unit. **Results:** In vitro measurements showed a strong correlation between the DSIAP and the reference ($r = 0.99$, p -value $< 2.2 \times 10^{-16}$). The bias and 95% confidence intervals were 0.135 and -0.821 - 1.091 cm H₂O, respectively. Measurements in patients with DSIAP versus Kron's method shown a very good correlation ($r = 0.973$, p -value $< 5.46 \times 10^{-13}$), while the bias and confidence intervals were 0.018 and -3.461 - 3.496 mmHg, respectively. **Conclusions:** The results suggest that the proposed DSIAP showed a profile similar to pressure transducers already in clinical use while overcoming some limitations of the former.

Key Words: Disposable sensor. Intra-abdominal pressure. Pressure transducer. Kron's method.

Resumen

Antecedentes: La medición de la presión intraabdominal (PIA) generalmente se realiza con el método de Kron, a pesar de presentar inconvenientes como la infusión de agua en la vejiga del paciente. **Objetivo:** Introducir un nuevo sensor desechable para medir la PIA (SDPIA) que aborda algunas limitaciones del método de Kron. **Método:** Se probó el SDPIA en pruebas in vitro y clínicas. La técnica se contrastó con el método de Kron empleando la correlación de Pearson y el análisis de Bland-Altman. Para las pruebas in vitro se realizaron 159 mediciones simulando la PIA en la vejiga. Para las pruebas clínicas se realizaron 20 mediciones en pacientes con monitorización rutinaria de la PIA en la unidad de cuidados intensivos. **Resultados:** En las mediciones in vitro se encontró una alta correlación ($r = 0.99$; $p < 2.2 \times 10^{-16}$). El sesgo para la diferencia entre los dos métodos de medición fue de 0.135 cm H₂O, con un intervalo de confianza del 95% de -0.821 a 1.091 cm H₂O. En las mediciones clínicas también se encontró una

Correspondencia:

*José S. Camacho-Juárez

Facultad de Ciencias

Avda. Parque Chapultepec, 1570

C.P. 78210, San Luis Potosí, S.L.P., México

E-mail: sergio_camacho@fc.uaslp.mx

Fecha de recepción: 20-09-2018

Fecha de aceptación: 26-06-2019

DOI: 10.24875/CIRU.19000756

Cir Cir. 2020;88(1):7-14

Contents available at PubMed

www.cirurgiaycirujanos.com

0009-7411/© 2019 Academia Mexicana de Cirugía. Publicado por Permanyer. Éste es un artículo open access bajo la licencia CC BY-NC-ND (<http://creativecommons.org/licenses/by-nc-nd/4.0/>).

Chloride-Induced Surface States in Cu(110)/Liquid Interfaces

Saul Vazquez-Miranda,* Raul E. Balderas-Navarro, Kurt Hingerl, and Christoph Cobet*

Cite This: *J. Phys. Chem. C* 2020, 124, 25403–25411

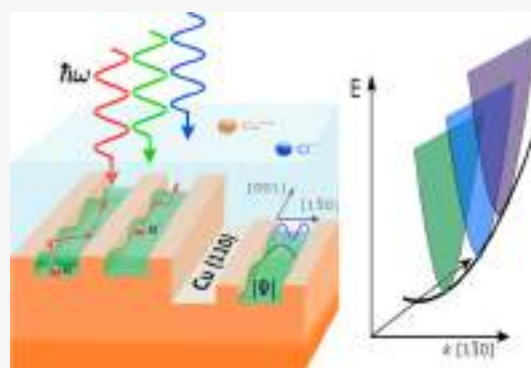
Read Online

ACCESS |

Metrics & More

Article Recommendations

ABSTRACT: While surface states (SSs) have been widely exploited under ultrahigh vacuum conditions, their appearance and role in metal–electrolyte interfaces are still a controversial debate. The existence of SSs, similar to those shown here, permits control and tunability of electronic properties of functional metal–electrolyte interfaces. Resonant excitations among them could enhance, for example, photocatalytic reactions or permit further investigations of the surface chemistry of such reactions with surface resonance Raman spectroscopy. On the one hand, SSs and other properties are readily adjustable via an applied electrical potential, that is, by promoting changes in the chemical potential favoring adsorption of ionic species. On the other hand, the presence of the electrolyte induces additional scattering and screening effects, so that the electron charge distributions can differ considerably in the presence of high electric fields as compared to the respective surfaces in vacuum. Hence, a straightforward comparison is challenging. In this work, we report on a systematic study, by means of electrochemical impedance spectroscopy (EIS) jointly with *in situ* reflectance anisotropy spectroscopy (RAS), which aimed to assess the evolution of surface properties and SSs occurring at Cu(110) in contact with an HCl solution. Thereafter, by modeling the RAS response and in comparison with electrochemical scanning tunneling microscopy measurements, specific surface structures have been identified and ascribed to the optical response. In a specific potential range, three additional resonances are detected in RAS that can be explained by two-dimensional confined SSs. This work renders both *in situ* RAS and EIS as useful tools to study and tune SSs in a systematic way by applied electrical potentials, thereby stabilizing thermodynamically preferred surface structures.



INTRODUCTION

The first identification of specific surface states (SSs) on noble metals was carried out with photoemission experiments in ultrahigh vacuum (UHV) and with supporting *ab initio* calculations.^{1,2} The ability to exploit polarized light in place of electrons gave researchers an additional way of probing fundamental interactions of SSs in non-UHV conditions. In this regard, the subject of SSs at the copper (110) surface was discussed in several previous publications. Of particular note is the pioneering work of Barritt and Weightman, et al. They have shown that reflection anisotropy spectroscopy (RAS) is a versatile optical probe to assess the formation of anisotropic surface properties of Cu(110) in electrolyte environments.^{3,4} However, the proposed interpretation of their experimental results poses some challenges. In this context, the controversially discussed results for Au(110) in electrolyte^{5,6} as well as the early work of Kolb et al. on Ag(100)⁷ should also be mentioned.

Certain spectral features in RAS have been unambiguously addressed to specific SSs,^{8–10} in the framework of the other experiments in UHV and with the supporting theoretical approaches. An identification of related electronic properties is considered to be more difficult for solid–liquid interfaces

because of the limited applicability of electron-based techniques. However, the theoretical *ab initio* attempts are also more demanding.

Results from *in situ* electrochemical scanning tunneling microscopy (EC-STM)^{11–13} and impedance spectroscopy, as presented in the following, indicate the complexity of the Cu(110) surface in hydrochloric acid (HCl) depending on the applied potentials. Possible reasons for misinterpretations arise from the high sensitivity of the surface to oxygen¹⁴ which will be considered in more detail in a subsequent publication. In ref 12, we have discussed by means of EC-STM the step-wise transformation of the Cu(110) surface from the pristine state, showing the 1 × 1 structure of the uppermost copper surface atoms, toward a faceted surface because of the increasing anodic potentials and chloride adsorption. The latter facets were also observed upon Cl[−] deposition in UHV.¹⁵ At

Received: September 3, 2020

Revised: October 26, 2020

Published: November 10, 2020



Adsorbate Isotherm Analysis by Reflection Anisotropy Spectroscopy on Copper (110) in Hydrochloric Acid

Saul Vazquez-Miranda,* Vladyslav Solokha, Raul E. Balderas-Navarro, Kurt Hingerl, and Christoph Cobet*

Cite This: *J. Phys. Chem. C* 2020, 124, 5204–5212

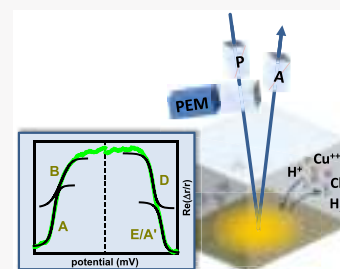
Read Online

ACCESS |

Metrics & More

Article Recommendations

ABSTRACT: Reflectance anisotropy spectroscopy (RAS) is a powerful optical probe that works on a polarization contrast basis. It can be operated in any environment, ranging from ultrahigh vacuum to vapor phases and liquids. The measured optical anisotropies are caused by several symmetry breaking effects and are exclusively assigned to the surface for otherwise bulk isotropic materials. In this work, we present a systematic study comprising in situ RAS-transient to assess the surface thermodynamics of the chloride adsorption on Cu(110) upon systematic variations of the applied electrode potentials in comparison to cyclic voltammetry (CV). Numerical time-derivatives of the measured RAS-transients are shown to be exclusively associated with electrical currents of those electrochemical reactions, which change the properties of the electrode surface. The recorded transient line-shapes track the Frumkin type isotherm properties related to chloride coverage. Both connections are theoretically discussed. Owing to the surface and interface specificity, RAS is shown to exhibit a high surface sensitivity. In particular, processes taking place in parallel, namely, the hydrogen evolution reaction (HER) as well as the copper dissolution as Cu^+ and Cu^{2+} , do not contribute to the RAS response.



1. INTRODUCTION

When foreign ions or molecules adsorb on metals they cause changes in their surfaces. Such surface modifications are complex and deserve detailed studies in any environment. As a matter of fact, in ultrahigh vacuum (UHV), molecular chlorine (Cl_2) adsorption on Cu(110) has been extensively studied with scanning tunneling microscopy (STM) and low energy electron diffraction (LEED).^{1,2} In liquid environments, atom species are prone to alter the liquid-metal interface in a different way; i.e., ions are adsorbed instead of neutral atoms and molecules. In electrochemical conditions, for instance, electron-based probes (like LEED) are clearly incompatible, and therefore noninvasive analytical techniques are much preferred. Photonic probes (PP) have been employed because they use light and are transparent to the liquid hosting the metal surface. However, as the heart of the reaction mechanism stems mainly from the surface region, PPs need to exploit an anisotropic surface in order to retrieve information solely from the surface, filtering out the isotropic, albeit dominant, bulk contribution.³ One of such linear optical probes is termed reflectance anisotropy spectroscopy (RAS), which measures the optical anisotropies through a contrast of two in-plane orthogonal crystallographic directions. This is advantageous when dealing with low index metal surfaces which are chemically more active to adsorption phenomena. In particular, the Cu(110) surfaces have been exploited under several conditions,^{4,5} including electrochemical (EC) reaction regimes.^{6–9}

In this paper, we demonstrate the power of RAS as an analytical probe capable to measure the complex reaction of chlorine ions Cl^- adsorption on low index metal surfaces. Special attention is paid to the possibility of quantifying certain surface structures and deriving respective thermodynamic potentials. In a previous work, we showed by EC-STM that the Cu(110) surface structures change in several steps due the anodic adsorption of chloride.^{7,9} Most prominent is the formation of a stripe/groove-structures in the [001] surface direction. The latter are about 2.6 nm wide and keep a minimum distance of the same order. A second major surface oxidation step results in a faceting of the surface. When using the appropriate photon energy, in operando kinetic RAS is able to detect electroadsorption isotherms of the Frumkin type for this Cl^- induced structuring.

The relationship between the polarization optical response as determined with RAS and the adsorbate induced surface structures, on one hand, and the currents measured (e.g., in cyclic voltammetry (CV)), on the other hand, needs to be clarified first. The rest of the paper is organized as follows. In the **Theory** section, we summarize first the conceptual approach and review approximations made therein. In the





Received: December 6, 2019

Revised: January 31, 2020

Published: February 5, 2020

Review

Emerging Optical Techniques for the Diagnosis of Onychomycosis

Chrysoula Petrokilidou ¹, Georgios Gaitanis ², Ioannis D Bassukas ² , Aristeia Velegraki ^{3,4}, Edgar Guevara ⁵ , Martha Z Vardaki ¹  and Nikolaos Kourkoumelis ^{1,*} 

¹ Department of Medical Physics, School of Health Sciences, University of Ioannina, 45110 Ioannina, Greece; chrisa_pe@hotmail.com (C.P.); martha.vardaki@mssl.ubc.ca (M.Z.V.)

² Department of Skin & Venereal Diseases, School of Health Sciences, University of Ioannina, 45110 Ioannina, Greece; ggaitan@uoi.gr (G.G.); ibassuka@uoi.gr (I.D.B.)

³ Mycology Research Laboratory & UOA/HCPF Culture Collection, 15772 Athens, Greece; aveleg@med.uoa.gr

⁴ Biomedicine SA, 11526 Athens, Greece

⁵ CONACYT-Universidad Autónoma de San Luis Potosí, 78210 San Luis Potosí, Mexico; eguevara@conacyt.mx

* Correspondence: nkourkou@uoi.gr

Received: 14 February 2020; Accepted: 24 March 2020; Published: 29 March 2020



Abstract: Onychomycosis is the most prevalent nail infection. Although it is not a life-threatening condition, it impacts the quality of life for many patients and often imposes a challenging diagnostic problem. The causative agents are dermatophytes, yeasts and non-dermatophytic moulds. Accurate and early diagnosis, including the identification of the causative species, is the key factor for rational therapy. Still, early diagnosis is not optimal as the current gold standard for the differentiation of the infectious agents is culture-based approaches. On the other hand, noninvasive optical technologies may enable differential diagnosis of nail pathologies including onychomycosis. When light penetrates and propagates along the nail tissue, it interacts in different ways with the components of either infected or healthy nail segments, providing a wealth of diagnostic information upon escaping the tissue. This review aims to assess alternative optical techniques for the rapid diagnosis of onychomycosis with a potential to monitor therapeutic response or even identify the fungal agent non-invasively and in real time in a clinical setting.

Keywords: onychomycosis; nails; keratin; Raman spectroscopy; OCT; confocal microscopy

1. Introduction

Onychomycosis is a common, chronic, highly-relapsing fungal nail infection that affects primarily the toenails [1]. It can impact the structural integrity of the whole nail, the matrix, bed, and nail plate. Despite being a non-life-threatening condition, onychomycosis influences the patients' quality of life due to disfigurement and pain. Additionally, the relation to immunosuppression and other co-morbidities, like diabetes mellitus [2], upgrades onychomycosis to a significant medical condition rather than a mere aesthetic problem. Fungal infections represent almost 50% of all nail conditions [3] with a prevalence varying between 3% and 26% in different populations around the world (4.3% across Europe and North America) [4]. Principal causative agents of onychomycosis are the dermatophytes, particularly *Trichophyton rubrum*, followed by yeasts (predominantly *Candida* species). The dermatophytes are specialized pathogenic fungi that digest the hard keratin of nail tissues into short peptides and amino acids which are further assimilated by the fungi via selective membrane transporters, ultimately leading to brittle and damaged nails [5]. A main structural component of keratins are cysteine moieties which confer chemical stability and tissue rigidity through crosslinking of disulphide bonds. The



An improved visually meaningful encrypted image scheme

J.O. Armijo-Correa^a, J.S. Murguía^{b,*}, M. Mejía-Carlos^c, V.E. Arce-Guevara^b,
J.A. Aboytes-González^c

^a Facultad de Ciencias, Universidad Autónoma de San Luis Potosí, Álvaro Obregón 64, 78000 San Luis Potosí, S.L.P., Mexico

^b Laboratorio Nacional CI3M, Facultad de Ciencias, Universidad Autónoma de San Luis Potosí, Álvaro Obregón 64, 78000 San Luis Potosí, S.L.P., Mexico

^c Instituto de Investigación en Comunicación Óptica, Universidad Autónoma de San Luis Potosí, Álvaro Obregón 64, 78000 San Luis Potosí, S.L.P., Mexico

HIGHLIGHTS

- An improved visually meaningful image encryption scheme is described.
- The scheme presents a high visual security of cipher image.
- The two-dimensional detrended fluctuation analysis is used as an objective measure of the quality of encryption procedures.
- Most of the times, this scheme outperforms some existing schemes.

ARTICLE INFO

Keywords:

Image encryption
Visually meaningful encrypted image
S-box
Integer discrete wavelet transform

ABSTRACT

An encrypted image generally presents an appearance of texture-like or noise-like image, which exhibits an indication of encrypted data that may motivate a significantly large number of attacks. To address this problem several approaches have been carried out, where an encrypted image is transformed into a visually meaningful encrypted image (VMEI). We present an improved approach to encrypt a plain image into a visually meaningful cover image, where the preprocessing and embedding phases are modified to achieve a quite comparable performance. To make the assessment of this proposal, some standard metrics such as PSNR and SSIM are performed, and the obtained numerical results show that this proposal is comparable or superior to some VMEI schemes used as benchmark in this work. In most of the reference images considered in the dataset the values of PSNR are greater than 40 dB, and a value close to 1 for the SSIM metric, which means a great similarity and high quality, respectively, between the reference images and their obtained VMEI images. Also, the two-dimensional detrended fluctuation analysis is carried out to observe the scaling behavior of the images, which allows us to have a perceptual security parameter of encrypted images and visually meaningful cover images. For this metric, the scaling exponent values of the VMEI images are close to 2.1, which are very similar to the values obtained for the reference images, a situation that confirms that the hidden information may not be detected by the human visual system. Furthermore, for two reference images, this metric was able to detect how the pixel values are distributed, and how the pixel values are highly correlated, suggesting that this metric can be an objective measure of encrypted images.

1. Introduction

With the recent advances in technology, digital communications have evolved dramatically in these years to such a level that it is hard to imagine a normal life without them. For instance, many people necessarily require the usage of cloud and internet-based services across the world to handle and share multimedia data such as documents, audio, image and video. Some of the data may contain private, important or classified information that requires protection from an

unauthorized access. To overcome this problem, several encryption systems based on different approaches are available, such as Advanced Encryption Standard (AES), International Data Encryption Algorithm (IDEA), Encryption System based on Cellular Automata (ESCA), among others [1,2]. Many encryption systems are generally used for encrypting textual data, but they present a poor performance for images, due to some intrinsic features, such as high redundancy, bulk data capacity, high correlation among pixels, and others. Thus, the correct choice of a particular encryption system will depend on the type of

* Corresponding author.

E-mail address: ondeleto@uaslp.mx (J.S. Murguía).

<https://doi.org/10.1016/j.optlastec.2020.106165>

Received 6 September 2019; Received in revised form 10 January 2020; Accepted 24 February 2020

Available online 14 March 2020

0030-3992/ © 2020 Elsevier Ltd. All rights reserved.

Chapter

Semiconductor Surface State Engineering for THz Nanodevices

*Irving Eduardo Cortes-Mestizo, Edgar Briones,
Leticia Ithsmel Espinosa-Vega and Victor Hugo Mendez-García*

Abstract

This chapter is dedicated to study the semiconductor surface states, which combined with nanolithography techniques could result on remarkable properties of advanced nanodevices suitable for terahertz (THz) signal detection or harvesting. The author presents the use of low-dimensional semiconductor heterostructures for the development of the so-called self-switching diodes (SSDs), studying by simulation tool key parameters in detail such as the shape and size of the two-dimensional electron gas system. The impact of the geometry on the working principle of the nanodevice and the effects on current-voltage behavior will be described in order to acquire design guidelines that may improve the performance of the self-switching diodes when applied to low-power square-law rectifiers as well as elements in rectennas by appropriately setting the size of the components.

Keywords: surface states engineering, self-switching diode, L-shape, V-shape, W-shape, rectenna

1. Introduction

The terahertz frequency range of the electromagnetic spectrum represents a technology gap between the electronic and optical well-stabilized technologies. Thus, the obtention of systems designed to generate, detect, and process THz radiation still is of scientific attention by the full of potential applications. Meanwhile sources available nowadays are typically expensive, fallible, and voluminous. It is possible to extend the electronic and optic concepts, for the THz radiation with millimetric and micrometric wavelength, respectively. However, the use of electronic in the THz range needs small circuits and high-frequency cutoff, while optical requests deal with the dimensions necessities to work in the THz range [1].

Electronic has been one of the most advanced technologies applied in the modern life, being imperative to extend the electronic concepts such as resistance, diode, and transistor to operate in the THz range with the aim to fill the so-called THz gap by small, efficient, and low-cost technologies. The use of electronic devices in THz implies both high carriers' mobility and short flight time of carriers between electrodes. The nanodevices are one of the most promising alternatives to the development of the THz technology. Recently, the semiconductor nanodevices have been employed for the generation and detection of THz radiation [1–6] showing an enormous potential for their application.



GaAs/InGaAs heterostructure strain effects on self-assembly of InAs quantum dots

C.A. Mercado-Ornelas^a, I.E. Cortes-Mestizo^b, E. Eugenio-López^{a,g}, L.I. Espinosa-Vega^a, D. García-Compean^b, A. Yu. Gorbachev^d, L. Zamora-Peredo^e, C.M. Yee-Rendon^f, V.H. Méndez-García^{a,*}

^a Center for the Innovation and Application of Science and Technology, Universidad Autónoma de San Luis Potosí (UASLP), Av. Sierra Leona #550, Col. Lomas 2a Sección, 78210, San Luis Potosí, Mexico

^b CONACYT-Center for the Innovation and Application of Science and Technology, Universidad Autónoma de San Luis Potosí (UASLP), Av. Sierra Leona #550, Col. Lomas 2a Sección, 78210, San Luis Potosí, Mexico

^c Departamento de Ingeniería Eléctrica, Electrónica y Mecatrónica, Tecnológico Nacional de México-Instituto Tecnológico de San Luis Potosí, Mexico

^d Optical Communications Research Institute, Universidad Autónoma de San Luis Potosí, Av. Karakorum #1470, Lomas 4a Secc. C.P. 78210, San Luis Potosí, Mexico

^e Centro de Investigación en Micro y Nanotecnología, Boca del Río, Veracruz, Mexico

^f Facultad de Ciencias Físico-Matemáticas, Universidad Autónoma de Sinaloa, Culiacán, Sinaloa, Mexico

^g Zentrum für Oberflächen-und Nanoanalytik Johannes Kepler University, Linz, Austria

ARTICLE INFO

Keywords

InAs quantum dots
InGaAs tensor layer
Modulating strain layer
Strain distribution
Strain modulation

ABSTRACT

In this study, the quantum dots (QDs) self-assembly properties were affected by strain modulation. The strain of the GaAs (100) surface was modulated prior to the growth of InAs with the aim to tailor the size and distribution of self-assembled QDs. Changes in the strain fields were achieved with the buried GaAs/InGaAs heterostructure by varying the GaAs layer thickness Σ , which significantly influences several parameters collectively involved in the QDs self-assembly process. In situ characterization of the heterostructure shows that the InAs/GaAs critical thickness and the surface diffusion parameter, the latter of which is an indicative of the QDs density, decreased with Σ . High-resolution X-ray diffraction measurements confirmed that depending on Σ , the InGaAs layer can be partially relaxed, presumably through the introduction of dislocations that are advanced by the QDs strain. Numerical simulations of the heterostructures were performed, with the sample's geometry and other properties obtained from its experimental characterization as input data. The results confirmed variations in strain resulting from changes in the GaAs/InGaAs heterostructure. These findings contribute to the understanding of strain distribution and can thus lead to improvements in the self-assembly properties of InAs QDs.

1. Introduction

Self-assembled quantum dots (QDs) have been attracting significant attention in the past years owing to their potential application in the development of unique electronic and optoelectronic devices, which demonstrated the capability to increase the performance of several current technologies [1,2]. For example, the performance of nano-devices such as the high electron mobility transistor (HEMT), high-efficiency LEDs, lasers, IR-detectors, and energy storage devices have been enhanced by implementation of QDs nanostructures [2–4]. Special attention has been given to the development of photovoltaic devices, where the interband is realized by embedding a stack of QDs within a conventional p-n junction solar cell. In this class of photovoltaics, the quantized energy levels of the QDs generate an extended photoreponse for wavelengths below the p-n based-material energy band gap, exhibiting a theoretical limit of energy conversion efficiency at approximately 63% [5–7]. The upsurge in the absorption efficiency supported by sub-

band transitions is explored by adequate control of energy levels exhibited by QDs, along with the increase in the number of the layers that can be grown without deteriorating the crystalline heterostructure. According to this concept, the properties and characteristics of the shape and size of QDs must be carefully designed for any device application, as these parameters dictate the allowed energy states and transitions that control optical and electrical behavior. In this light, numerous methods have been proposed to tailor the QD dimensions, such as altering substrate orientation, varying growth parameters, changing band discontinuity between QDs and barriers layers, etc. [5,8,9]. The most conventional method applied to self-assemble QDs by molecular beam epitaxy (MBE) is the Stranski-Krastanov growth mode, which is a mechanism mainly governed by strain [8,9]. Thus, by modulating the strain in samples prior to the QDs growth, it is possible to control their shape, size, and distribution. However, during the growth of multi-stacked QDs structures, residual compressive strain is accumulated on each layer, which might culminate in the alteration of crystal quality in

* Corresponding author.

E-mail address: victor.mendez@uaslp.mx (V.H. Méndez-García)



Overlapping effects of the optical transitions of GaNAs thin films grown by molecular beam epitaxy

I.E. Cortes-Mestizo^{a,*}, L.I. Espinosa-Vega^b, J.A. Espinoza-Figueroa^b, C.M. Yee-Rendón^c,
L. Zamora-Peredo^d, A.G. Rodríguez^b, C.A. Mercado-Ornelas^b, F.E. Perea-Parrales^b,
V.H. Méndez-García^b

^a CONACYT- Coordinación para la Innovación y la Aplicación de la Ciencia y la Tecnología (CIACYT), Universidad Autónoma de San Luis Potosí, Av. Sierra Leona #550, Col. Lomas 2a Sección, San Luis Potosí, San Luis Potosí, 78210, México

^b Coordinación para la Innovación y la Aplicación de la Ciencia y la Tecnología (CIACYT), Universidad Autónoma de San Luis Potosí, Av. Sierra Leona #550, Col. Lomas 2a Sección, San Luis Potosí, San Luis Potosí, 78210, México

^c Facultad de Ciencias Físico-Matemáticas, Universidad Autónoma de Sinaloa, Av. de las Americas y Blvd. Universitarios, Culiacán, Sinaloa, 80000, México

^d Centro de Investigación en Micro y Nanotecnología, Universidad Veracruzana, Calzada Ruiz Cortines #455, Boca del río, Veracruz, 94294, México

ARTICLE INFO

Keywords:

Gallium arsenide nitride
Conduction band splitting
Photoreflectance
Ellipsometry
Molecular beam epitaxy
GaNAs/GaAs heterojunction
Band anti-crossing model
Dilute nitride

ABSTRACT

Photoreflectance and ellipsometry are two very useful optical spectroscopy techniques employed to analyze the electronic band structure of semiconductors. Photoreflectance and ellipsometry spectra of gallium arsenide nitride (GaNAs) thin films on gallium arsenide (GaAs) layers may be composed of transitions from the conduction bands of the alloy and the binary (E_c , E_{c+} , and E_{c0} , respectively) in conjunction with their interaction spin-orbit split-off valence band ($E_v + \Delta_0$ and $E_{v0} + \Delta_0$). For low concentration of nitrogen (between 0.2 and 0.6 %), the determination of the E_{c+} conduction band becomes difficult to distinguish by the fact that critical points are superimposed in the spectrum of both characterization techniques. In this work, a method to determine the E_{c+} conduction band of GaNAs thin films grown on GaAs by molecular beam epitaxy is proposed when the overlapping of spectral features influences their optical determination. When using spectroscopic characterization techniques, the modulation/excitation region depends on the wavelength employed and sample characteristics, and consequently low nitrogen concentration in the alloy in conjunction with the thickness of the GaNAs layers have been found responsible for the signal overlapping. It is demonstrated that by decreasing the sample temperature in the photoreflectance process the overlapping is avoided, allowing for a correct interpretation of the GaNAs conduction band splitting analysis and discarding the contribution of built-in electric fields. From these results, we achieved a precise experimental determination of the presence/absence of the band splitting predicted by the band anti-crossing model using non-destructive characterization tools.

1. Introduction

Through the substitution of arsenic by nitrogen atoms in the gallium arsenide (GaAs) host lattice the gallium arsenide nitride ($\text{GaN}_x\text{As}_{1-x}$, where x is the mole fraction of N) ternary compound is formed. This material has been widely researched due to the attractive large bandgap bowing observed even for small atomic percentage of nitrogen (%N) incorporation since it was experimentally demonstrated in the early 1990s [1]. For instance, within the diluted regime (%N < 3) the band gap energy is reduced by ~ 100 meV per %N [2]. On this way, the development of the GaNAs has been a subject of great interest due to the potential applications in optoelectronic devices, covering emission/

absorption processes between red to ultraviolet [3-6].

The behavior of the band structure of the GaNAs system is explained by the band anti-crossing model (BAC), which describes the role of nitrogen incorporation on a wide variety of III-N-V alloys. The BAC indicates that anti-crossing interaction between the electronic states of the localized nitrogen and energy states of the GaAs host matrix split the conduction band into two sub-bands labeled as E_c and E_{c+} [7]. The band gap of the GaNAs system is related to E_c while the E_{c+} level is an extra conduction-band edge of the GaNAs. Thus, the $\text{GaN}_x\text{As}_{1-x}$ bandgap can be tuned in by the %N used in the alloy, according to BAC. As it was mentioned earlier, a small increment of %N decreases the bandgap energy, E_c , while at the same time increases the energy separation

* Corresponding author.

E-mail address: irving.cortes@uaslp.mx (I.E. Cortes-Mestizo).

<https://doi.org/10.1016/j.tsf.2020.137969>

Received 12 September 2019; Received in revised form 7 February 2020; Accepted 18 March 2020

Available online 20 March 2020

0040-6090/ © 2020 Elsevier B.V. All rights reserved.



An improved visually meaningful encrypted image scheme

J.O. Armijo-Correa^a, J.S. Murguía^{b,*}, M. Mejía-Carlos^c, V.E. Arce-Guevara^b,
J.A. Aboytes-González^c

^a Facultad de Ciencias, Universidad Autónoma de San Luis Potosí, Álvaro Obregón 64, 78000 San Luis Potosí, S.L.P., Mexico

^b Laboratorio Nacional CI3M, Facultad de Ciencias, Universidad Autónoma de San Luis Potosí, Álvaro Obregón 64, 78000 San Luis Potosí, S.L.P., Mexico

^c Instituto de Investigación en Comunicación Óptica, Universidad Autónoma de San Luis Potosí, Álvaro Obregón 64, 78000 San Luis Potosí, S.L.P., Mexico

HIGHLIGHTS

- An improved visually meaningful image encryption scheme is described.
- The scheme presents a high visual security of cipher image.
- The two-dimensional detrended fluctuation analysis is used as an objective measure of the quality of encryption procedures.
- Most of the times, this scheme outperforms some existing schemes.

ARTICLE INFO

Keywords:

Image encryption
Visually meaningful encrypted image
S-box
Integer discrete wavelet transform

ABSTRACT

An encrypted image generally presents an appearance of texture-like or noise-like image, which exhibits an indication of encrypted data that may motivate a significantly large number of attacks. To address this problem several approaches have been carried out, where an encrypted image is transformed into a visually meaningful encrypted image (VMEI). We present an improved approach to encrypt a plain image into a visually meaningful cover image, where the preprocessing and embedding phases are modified to achieve a quite comparable performance. To make the assessment of this proposal, some standard metrics such as PSNR and SSIM are performed, and the obtained numerical results show that this proposal is comparable or superior to some VMEI schemes used as benchmark in this work. In most of the reference images considered in the dataset the values of PSNR are greater than 40 dB, and a value close to 1 for the SSIM metric, which means a great similarity and high quality, respectively, between the reference images and their obtained VMEI images. Also, the two-dimensional detrended fluctuation analysis is carried out to observe the scaling behavior of the images, which allows us to have a perceptual security parameter of encrypted images and visually meaningful cover images. For this metric, the scaling exponent values of the VMEI images are close to 2.1, which are very similar to the values obtained for the reference images, a situation that confirms that the hidden information may not be detected by the human visual system. Furthermore, for two reference images, this metric was able to detect how the pixel values are distributed, and how the pixel values are highly correlated, suggesting that this metric can be an objective measure of encrypted images.

1. Introduction

With the recent advances in technology, digital communications have evolved dramatically in these years to such a level that it is hard to imagine a normal life without them. For instance, many people necessarily require the usage of cloud and internet-based services across the world to handle and share multimedia data such as documents, audio, image and video. Some of the data may contain private, important or classified information that requires protection from an

unauthorized access. To overcome this problem, several encryption systems based on different approaches are available, such as Advanced Encryption Standard (AES), International Data Encryption Algorithm (IDEA), Encryption System based on Cellular Automata (ESCA), among others [1,2]. Many encryption systems are generally used for encrypting textual data, but they present a poor performance for images, due to some intrinsic features, such as high redundancy, bulk data capacity, high correlation among pixels, and others. Thus, the correct choice of a particular encryption system will depend on the type of

* Corresponding author.

E-mail address: ondeleto@uaslp.mx (J.S. Murguía).

<https://doi.org/10.1016/j.optlastec.2020.106165>

Received 6 September 2019; Received in revised form 10 January 2020; Accepted 24 February 2020

0030-3992/ © 2020 Elsevier Ltd. All rights reserved.

SCALING ANALYSIS OF THE A-PHASE DYNAMICS DURING SLEEP

V. E. ARCE-GUEVARA,* M. O. MENDEZ,[†] J. S. MURGUÍA,*[‡] A. ALBA,*
H. GONZÁLEZ-AGUILAR,* and E. R. PALACIOS-HERNÁNDEZ*

**Laboratorio Nacional CI3M, Facultad de Ciencias
Facultad de Ciencias, Universidad Autónoma de San Luis Potosí (UASLP)
Alvaro Obregón 64, 78000 San Luis Potosí, S.L.P., Mexico*

*[†]Laboratorio Nacional CI3M, Facultad de Ciencias & CICSaB
Universidad Autónoma de San Luis Potosí (UASLP)
Alvaro Obregón 64, 78000 San Luis Potosí, S.L.P., Mexico*

[‡]ondeleto@uaslp.mx

Received March 14, 2017
Accepted December 17, 2019
Published March 31, 2020

Abstract

In this work, the scaling behavior of the sleep process is evaluated by using detrended fluctuation analysis based on wavelets. The analysis is carried out from arrivals of short and recurrent cortical events called A-phases, which in turn build up the Cyclic Alternating Pattern phenomenon, and are classified in three types: A1, A2 and A3. In this study, 61 sleep recordings corresponding to healthy, nocturnal frontal lobe epilepsy patients and sleep-state misperception subjects, were analyzed. From the A-phase annotations, the onsets were extracted and a binary sequence with one second resolution was generated. An item in the sequence has a value of one if an A-phase onset occurs in the corresponding window, and a value of zero otherwise. In addition, we consider other different temporal resolutions from 2s to 256s. Furthermore, the same analysis was carried out for sequences obtained from the different types of A-phases and their combinations. The results of the numerical analysis showed a relationship between the time resolutions and the scaling exponents; specifically, for higher time resolutions a white noise behavior is observed, whereas for lower time resolutions a behavior towards to $1/f$ -noise is

[‡]Corresponding author.



STABILITY, COHOMOLOGY VANISHING, AND NONAPPROXIMABLE GROUPS

MARCUS DE CHIFFRE¹, LEV GLEBSKY², ALEXANDER LUBOTZKY³
and ANDREAS THOM⁴

¹ TU Dresden, Germany;

email: marcus@dechiffre.dk

² L.G., Universidad Autónoma de San Luis Potosí, México;

email: glebsky@cactus.iico.uaslp.mx

³ A.L., Hebrew University, Israel;

email: alex.lubotzky@mail.huji.ac.il

⁴ TU Dresden, Germany;

email: andreas.thom@tu-dresden.de

Received 28 March 2019; accepted 20 December 2019

Abstract

Several well-known open questions (such as: are all groups sofic/hyperlinear?) have a common form: can all groups be approximated by asymptotic homomorphisms into the symmetric groups $\text{Sym}(n)$ (in the sofic case) or the finite-dimensional unitary groups $U(n)$ (in the hyperlinear case)? In the case of $U(n)$, the question can be asked with respect to different metrics and norms. This paper answers, for the first time, one of these versions, showing that there exist finitely presented groups which are *not* approximated by $U(n)$ with respect to the Frobenius norm $\|T\|_{\text{Frob}} = \sqrt{\sum_{i,j=1}^n |T_{ij}|^2}$, $T = [T_{ij}]_{i,j=1}^n \in M_n(\mathbb{C})$. Our strategy is to show that some higher dimensional cohomology vanishing phenomena implies *stability*, that is, every Frobenius-approximate homomorphism into finite-dimensional unitary groups is close to an actual homomorphism. This is combined with existence results of certain nonresidually finite central extensions of lattices in some simple p -adic Lie groups. These groups act on high-rank Bruhat–Tits buildings and satisfy the needed vanishing cohomology phenomenon and are thus stable and not Frobenius-approximated.

2010 Mathematics Subject Classification: 22D10 (primary); 39B82 (secondary)



On the usefulness of the equation of state approach for contact angles on rough surfaces

G. Sánchez-Balderas¹ · Elías Pérez¹

Received: 23 August 2019 / Accepted: 25 November 2019
© Springer-Verlag GmbH Germany, part of Springer Nature 2019

Abstract

The equation of state (EQS) approach has been used successfully to calculate the surface tension of solids for flat surfaces where only the effects of the tensions involved are dominant and define the wettability. In this work we use the EQS approach to modelate the wetting by ethylene glycol, glycerol, and water on homogeneous polymer rough surfaces. The surfaces were made of polystyrene using the phase separation method and topographically characterized by atomic force microscopy through the area factor (r_a). We also defined an *effective* surface tension γ'_{sv} , which decreases with the roughness and it explains the increasing of the contact angle for these surfaces.

1 Introduction

Surface wetting is defined by the liquid contact angle (usually water) on the surface, and it has been the subject of numerous studies for many decades [1]. The contact angle is used in many scientific, technological and industrial problems that concern the solid–liquid interface [2]. As is known, the equilibrium contact angle (θ_Y) for liquid drop on a flat homogeneous surface is given by Young's equation [3, 4]

$$\gamma_{lv} \cos \theta_Y = \gamma_{sv} - \gamma_{sl}, \quad (1)$$

where γ_{lv} , γ_{sv} and γ_{sl} are the liquid–vapor, solid–vapor, and solid–liquid interfacial tensions, respectively. Even though γ_{lv} and θ_Y can be easily evaluated [5], this is not the case for the other two surface tensions, which are difficult to determine directly [6]. Additionally, Young's equation is no longer valid for rough and inhomogeneous surfaces. Instead, Wenzel and Cassie–Baxter have proposed alternative equations that take into account the roughness (Wenzel) and inhomogeneity (Cassie–Baxter). For instance, Wenzel assumed that the roughness of the surface increases the solid–liquid interfacial tensions by a factor, r_a , which is the ratio between the actual wetting area and the flat area [3, 7]. In this case, Wenzel's contact angle θ_W is given by [8]

$$\cos \theta_W = r_a \cos \theta_Y. \quad (2)$$

The main criticism of Wenzel's equation is the assumption that the actual wetting area determines the contact angle [3, 9], which is not satisfactorily fulfilled. Gao and McCarthy [9–11] measured advancing and receding contact angles with water drops in different surfaces with smoother, rougher or spots chemically different from the surrounding field and showed that the Wenzel and Cassie–Baxter equations do not satisfy water repellency. They proposed that the contact line controls the contact angle [11], which means that wetting is explained using the surface tensions along the contact line [11–13]. An alternative description of the contact angle is given by the thermodynamic approach, where the interfacial tensions are related by an equation of state [1, 3, 4, 14–16], that allows predicting γ_{sv} and γ_{sl} from the contact angle. In this way, the cosine of the contact angle changes smoothly with the variation of the liquid–vapor interfacial tensions. In this approach the solid–liquid interfacial tension can be related by an equation of state [14, 15],

$$\gamma_{sl} = \gamma_{sv} - f(\gamma_{lv}, \gamma_{sv}) = F(\gamma_{lv}, \gamma_{sv}), \quad (3)$$

where f and F are unknown functions. A first approximation of this relation is given by the well-known geometric mean according to Berthelot's rule, where the solid–liquid interfacial tension is expressed as [4, 14, 17, 18]

$$\gamma_{sl} = \gamma_{lv} + \gamma_{sv} - 2\sqrt{\gamma_{lv}\gamma_{sv}}, \quad (4)$$

✉ Elías Pérez
elias@ifisica.uaslp.mx

¹ Instituto de Física, Universidad Autónoma de San Luis Potosí, Av. Manuel Nava 6, 78290 San Luis Potosí, SLP, Mexico



Regeneration of titanate nanotubes by *Aspergillus niger* and *Penicillium* sp. under static conditions

Claudia M. Martínez¹ · Mariana Hinojosa-Reyes¹ · Idania DeAlba-Montero¹ · Ismael Acosta-Rodríguez² · Facundo Ruíz¹ · Luis H. Álvarez³

Received: 16 August 2019 / Accepted: 20 January 2020
© Springer Japan KK, part of Springer Nature 2020

Abstract

The adsorption of triphenylmethane dyes on the surface of nanostructured oxide materials has been successfully applied for the removal of dye from wastewater. Although this removal strategy does not generate harmful substances, the adsorption is not destructive and involves a phase transfer of pollutants to other secondary wastes. Due to these disadvantages, it is necessary to evaluate eco-friendly biological strategies to remove the adsorbed contaminants, to reuse them and to continue taking advantage of its adsorption capacity. Information concerning regeneration of nanostructured oxide material by biologic methods is currently unavailable. In the present study, the regeneration of titanate nanotubes (TNTs) was investigated and compared in the presence of two different fungal species: *Aspergillus niger* and *Penicillium* sp. Efficient regeneration of TNTs was achieved in the presence of both fungal species and no significant differences were observed. The adsorption capacity of the regenerated TNTs decreased by only 38 and 48% for *A. niger* and *Penicillium* sp., respectively. The UV–Vis, FTIR analysis, and TEM images confirmed the complete desorption of BF and the preservation of the tubular structure of TNTs. This study demonstrates that the regeneration of TNTs using biological activity could represent an efficient alternative over physico-chemical regeneration.

Keywords Regeneration of titanate nanotubes · *Aspergillus niger* · *Penicillium* sp. · Basic fuchsin · Decolorization

✉ Claudia M. Martínez
claudiam.martinezr@gmail.com

✉ Luis H. Álvarez
luis.alvarez@itson.edu.mx

Mariana Hinojosa-Reyes
kittyhinojosa@hotmail.com

Idania DeAlba-Montero
didania@hotmail.com

Ismael Acosta-Rodríguez
iacosta@uaslp.mx

Facundo Ruíz
facundo@fciencias.uaslp.mx

¹ Facultad de Ciencias, Universidad Autónoma de San Luis Potosí, Lateral Av. Salvador Nava Martínez S/N, Zona Universitaria, 78290 San Luis Potosí, SLP, Mexico

² Facultades de Ciencias Químicas, Universidad Autónoma de San Luis Potosí, Lateral Av. Salvador Nava Martínez S/N, Zona Universitaria, 78290 San Luis Potosí, SLP, Mexico

³ Departamento de Ciencias Agronómicas Y Veterinarias, Instituto Tecnológico de Sonora, 5 de febrero 818 Sur, 85000 Ciudad Obregón, Sonora, Mexico

Introduction

Due to rapid industrialization and urbanization, a lot of chemicals including dyes are discharged into the environment in the form of effluents after processing or without processing. Its release into the environment is undesirable due to serious environmental problems linked with the dyes and their breakdown products [1, 2]. In particulate, triphenylmethane dyes are used extensively in textile, paper, leather, food, and cosmetic industries. Among them, basic fuchsin (BF) is widely used as colouring agent for textile and leather materials and in the staining of collagen, muscle, mitochondria, and tubercle bacillus [3, 4]. This cationic triphenylmethane has a stable aromatic structure, and thus, can resist environmental degradation. Its ingestion may cause gastrointestinal irritation with nausea, vomiting, and diarrhea. Inhalation or ingestion may also cause irritation to the respiratory tract and damage to the organs such as blood, liver, spleen, and thyroid [5]. Due to their environmental recalcitrance, toxicity, carcinogenicity and unsightliness to humans and animals, its removal has become a



Mentha piperita as a natural support for silver nanoparticles: A new *Candida albicans* treatment



Marissa Robles-Martínez^a, Rosalba Patiño-Herrera^{b,*}, Francisco Javier Pérez-Vázquez^c,
Juan Martín Montejano-Carrizales^d, Juan Fernando Cárdenas González^e, Elías Pérez^d

^a Doctorado Institucional en Ingeniería y Ciencia de Materiales de la UASLP, Sierra Leona 530, San Luis Potosí S.L.P. 78210, Mexico.

^b Departamento de Ingeniería Química, Tecnológico Nacional de México/ Instituto Tecnológico de Celaya, Antonio García Cubas Pte #600 esq. Av. Tecnológico. Celaya, Guanajuato 38010, Mexico.

^c Coordinación para la Innovación y Aplicación de la Ciencia y la Tecnología (CIACYT), Universidad Autónoma de San Luis Potosí, San Luis Potosí, Mexico.

^d Instituto de Física, UASLP, Álvaro Obregón 64, San Luis Potosí S.L.P. 78000, Mexico

^e Unidad Académica Multidisciplinaria Zona Media, UASLP, Rioverde, San Luis Potosí 79617, Mexico

ARTICLE INFO

Keywords:

Mentha piperita
Silver nanoparticles
Solvent
Candida albicans
Antimycotic
Secondary metabolites

ABSTRACT

A new proposal of biocompatible support, *Mentha piperita* aqueous and ethanolic extract decorated with silver nanoparticles, was successfully proved against *C. albicans*. Silver nanoparticles (AgNPs) with average size of 20 ± 3 nm, were synthesized to decorate both types of extracts, resulting in variations on the AgNPs distribution on the extract, depending on the solvent nature. The antimycotic activity of ethanolic extract exceeds aqueous extract by 89%, while decorated supports were 80% higher than without AgNPs. The activity of *MpExt*_{aq}-AgNPs is lower than *MpExt*_{et}-AgNPs since the nanoparticles are immersed in the extract, avoiding the action against *C. albicans*, whereas the *MpExt*_{et}-AgNPs remain on the extract surface. *C. albicans* optical images showed dismembered cells without hyphae as a result of the treatment with *MpExt*_{et}-AgNPs. As the *MpExt*_{et} contains anthocyanins that were not found in *MpExt*_{aq}, it is concluded that this secondary metabolite must play an important role in antifungal activity.

1. Introduction

In the last three decades, 95% of the pathogen infections attributed to *Candida* species, approximately 150 species were identified, such as *Candida glabrata*, *Candida tropicalis*, *Candida parapsilosis*, *Candida krusei* and mainly *Candida albicans* (*C. albicans*). This last species is still the most common yeast found in humans, candidiasis infection ranks fourth in frequency in US hospitals [1]. *C. albicans* is a pleomorphic and opportunistic pathogen, and many of these species have been isolated from vegetables, soil, water, air and food; in some cases, they stay at regular skin biota and mucous membranes (mouth, vagina, respiratory tract, gastrointestinal tract, oropharynx, genitourinary system) on humans; however, it easily produces an infection that affects mucous membranes and skin because any tissue can be affected by generating several clinical aspects, each of them related directly to patient's immune system. Therefore a systemic candidiasis may occur, which it is generally acute or chronic and is usually a severe disease. It can also infect medical implants, producing infection in bloodstream and deep tissues [2]. Besides it is the most prevalent infective species in

vulvovaginal candidiasis, an affection that occurs at least once in the life of 75% of women [3]. Norgaard et al. have proposed that invasive candidiasis is not only a consequence of cancer patients' weakness, but it also implies cancer risk in the following years. The reason for this is that that some byproducts of candidiasis metabolism may favor the cancer development or metastatic processes [4]. As a complication of cancer and its treatment, candidiasis seems to raise the mortality rate. Mortality is even higher when *Candida* bloodstream infections are diagnosed, with mortality rates of 56 and 67%, at 30 and 100 days, respectively [5]. Recent findings demonstrate that *C. albicans* promotes cancer by different mechanisms: carcinogenic byproducts production, inflammation triggering, Th17 response induction and molecular mimicry [6]. Since *C. albicans* plays an important role in nosocomial infections, during cancer treatment, Candidiasis infection need to be controlled to avoid the pro-tumor effect of this species. It is then urgent to find a new treatment. Onychomycosis is a nail infective disorder caused mainly by the anthropophilic dermatophytes *Trichophyton rubrum* and *Trichophyton mentagrophytes*, and 10–15% of the cases are attributed to the non-dermatophyte molds *Scopulariopsis brevicaulis*,

* Corresponding author.

E-mail address: roos_ph@iqcelaya.itc.mx (R. Patiño-Herrera).

<https://doi.org/10.1016/j.colcom.2020.100253>

Received 26 November 2019; Received in revised form 26 February 2020; Accepted 27 February 2020

Available online 05 March 2020

2215-0382/ © 2020 Elsevier B.V. This is an open access article under the CC BY-NC-ND license (<http://creativecommons.org/licenses/by-nc-nd/4.0/>).



Biosynthesis and characterization of cadmium carbonate crystals by anaerobic granular sludge capable of precipitate cadmium

C.M. Martínez^{a,*}, M. Rivera-Hernández^a, Luis H. Álvarez^b, Ismael Acosta-Rodríguez^c, F. Ruíz^a, V.D. Compeán-García^{d,**}

^a Facultad de Ciencias, Universidad Autónoma de San Luis Potosí, Lateral Av, Salvador Nava Martínez S/N, Zona Universitaria, San Luis Potosí, SLP, 78290, Mexico

^b Departamento de Ciencias Agronómicas y Veterinarias, Instituto Tecnológico de Sonora, 5 de Febrero 818 Sur, Ciudad Obregón, Sonora, 85000, Mexico

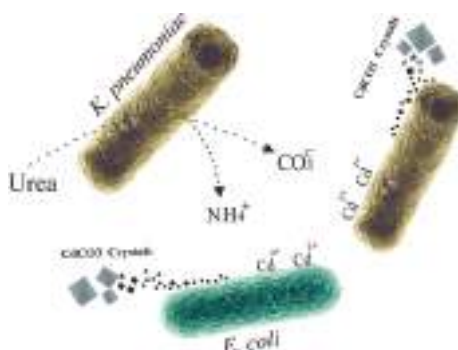
^c Facultad de Ciencias Químicas, Universidad Autónoma de San Luis Potosí, Lateral Av, Salvador Nava Martínez S/N, Zona Universitaria, San Luis Potosí, SLP, 78290, Mexico

^d CONACyT-Coordinación para La Innovación y Aplicación de La Ciencia y La Tecnología, Universidad Autónoma de San Luis Potosí, Sierra Leona #550, Lomas de San Luis, 78210, San Luis Potosí, Mexico

HIGHLIGHTS

- An anaerobic granular sludge was able to precipitation Cd^{2+} as CdCO_3 crystals.
- No differences were observed neither cadmium source nor substrate.
- Cd^{2+} precipitated as CdCO_3 rhombohedral crystals from 100 to 700 nm.
- Synthesis was associated to *K. pneumoniae* and *E. coli*.
- The co-precipitation of cadmium with other metals was not observed.

GRAPHICAL ABSTRACT



ARTICLE INFO

Keywords:

Cadmium precipitation
 CdCO_3 crystals characterization
 Anaerobic sludge
K. pneumoniae
E. coli

ABSTRACT

Microbially induced carbonate precipitation (MICP) has been exploited as an efficient strategy to immobilize toxic metals in the form of carbonate salts. The present study investigated the cadmium carbonate (CdCO_3) precipitation induced by an anaerobic granular sludge. The results revealed that anaerobic sludge showed high Cd utilization efficiencies ($97.4\% \pm 1.1$) after 18 h of incubation at 30°C , and no differences were observed neither cadmium source nor substrate. According to SEM and X-ray diffraction results, the anaerobic sludge was able to precipitate Cd^{2+} as CdCO_3 rhombohedral crystals in shape from 100 to 700 nm in size as a function of the source of cadmium and substrate used. FTIR results showed that 3 extra bands (1370 , 848 and 688 cm^{-1}) corresponding to CO_3^{2-} anion appeared once CdCO_3 was synthesized. TEM revealed the bioaccumulation of CdCO_3 on the bacterial cell wall and the synthesis of crystals smaller than 100 nm. The synthesis of CdCO_3 crystals was associated with *K. pneumoniae* and *E. coli*, which had a synergetic effect during CdCO_3 precipitation.

* Corresponding author.

** Corresponding author.

E-mail addresses: claudiam.martinezr@gmail.com (C.M. Martínez), Luna_Marix@hotmail.com (M. Rivera-Hernández), luis.alvarez@itson.edu.mx (L.H. Álvarez), iacosta@uaslp.mx (I. Acosta-Rodríguez), facundo@ciencias.uaslp.mx (F. Ruíz), damiancompean@gmail.com (V.D. Compeán-García).

<https://doi.org/10.1016/j.matchemphys.2020.122797>

Received 16 December 2019; Received in revised form 10 February 2020; Accepted 12 February 2020

Available online 14 February 2020

0254-0584/© 2020 Elsevier B.V. All rights reserved.



Structural and optical properties of gadolinium doped ZnTe thin films

J.D. López^{a,b,*}, L. Tirado-Mejía^a, H. Ariza-Calderón^a, H. Riascos^c, F. de Anda^d, E. Mosquera^{b,e}



^a Laboratorio de Optoelectrónica, Instituto Interdisciplinario de las Ciencias, Universidad del Quindío, A.A. 460, Colombia

^b Departamento de Física, Universidad del Valle, A.A. 25360, Cali, Colombia

^c Universidad Tecnológica de Pereira, Cra. 27 No 10-02, Pereira 660003, Risaralda, Colombia

^d Instituto de Investigación en Comunicación Óptica, UASLP, Av. Karakorum 1470, 78210 San Luis Potosí, Mexico

^e Centro de Excelencia en Nuevos Materiales, CENM, Universidad del Valle, A.A. 25360, Cali, Colombia

ARTICLE INFO

Article history:

Received 2 December 2019

Accepted 23 February 2020

Available online 24 February 2020

Keywords:

ZnTe

Thermal evaporation

Te-doped GaSb substrate

Thin films

ABSTRACT

ZnTe and Ga-doped ZnTe thin films were prepared onto glass and Te-doped GaSb substrates by thermal evaporation method under vacuum and their structural and optical properties were studied. XRD results show that for both substrates, the doping with gadolinium yield a reduction in the ZnTe lattice parameter. The optical band gap increases with incorporation of Gd into the ZnTe structure and the values obtained are 2.19 and 2.29 eV, respectively for glass and GaSb:Te substrates. The presence of defects due to Gd doping into ZnTe thin films is evidenced.

© 2020 Elsevier B.V. All rights reserved.

1. Introduction

Zinc Telluride (ZnTe) is one of the II-VI most attractive chalcogenides semiconductors employed for the development of optoelectronic devices such as blue light emitting diodes, solar cells and radiation detection [1–3]. ZnTe is usually a p-type semiconductor, with a direct band gap of 2.26 eV (~548 nm) at 300 K and a lattice constant of 6.103 Å [4]. Several methods have been developed for the preparation of ZnTe films such as liquid phase epitaxy (LPE), molecular beam epitaxy (MBE), thermal vapor deposition and pulsed laser deposition (PLD) [5–8]. With these methods, the choice of a substrate plays an important role in the deposition process, in particular for semiconductor diodes applications. Both ZnTe and Te-doped GaSb (GaSb:Te) with band gap of 0.814 eV at 11 K [9] have lattice constants close to 6.1 Å with a mismatch of only 0.13%. Also, the large difference in their refractive index leads an excellent optical confinement of the guided optical modes in semiconductor laser and others applications [10]. Therefore, several researchers have studied their structural, optical and electrical properties of In, Cu, Cr and Cd doped ZnTe films [11,12]. However, the structural and optical properties of thermal evaporated Gd-doped ZnTe (ZnTe:Gd) thin films has not been reported. Thus,

in this work, we present a study on structural and optical properties of thermally vacuum evaporate ZnTe and ZnTe:Gd thin films deposited onto glass and GaSb:Te substrates with potential application for medical and defense devices.

2. Experimental

For the ZnTe films, glass slides and GaSb:Te single crystal were used as substrates. Initially, glass substrates ($7.62 \times 2.54 \times 0.1 \text{ cm}^3$) were clean with a soap solution and rinsed with distilled water; after that, the substrates were submitted to ultrasonic agitation for 30 min in order to remove residual impurities. They were cleaned in boiling methanol, boiling acetone and isopropyl alcohol at room temperature (RT) for 10 min and dried with nitrogen. In the other hand, the preparation of GaSb:Te substrates were carried out by chemical etching performed with a H_2O_2 (3.5 mL):HF(125 μL): $\text{C}_4\text{O}_6\text{H}_6$ (7.5 mL): H_2O (2.35 mL) solution [13] during 5 min and then, the substrates were cleaned in boiling methanol, boiling acetone and isopropyl alcohol at RT for 10 min and dried with nitrogen.

ZnTe and ZnTe:Gd thin films were prepared using a vacuum coating unit: 12" \times 18" Pyrex Glass Bell Jar, rotary vane vacuum (Alcatel Pascal 2005 SD) for pre-vacuum, turbo-molecular high vacuum (Adixen Alcatel ATP), a current source, and a mechanical shutter. High purity powder of ZnTe (99,99%) and chips of Gd (99,9%) were used. The source-substrate distance was maintained at 13 cm and a rotary drive was employed to maintain uniformity in film thickness. The ZnTe (101 mg) powder were placed into a tantalum boat and it was heated indirectly by passing current

* Corresponding author at: Departamento de Física, Universidad del Valle, A.A. 25360, Cali, Colombia

E-mail addresses: jeison.lopez@correounivalle.edu.co (J.D. López), litirado@uniquindio.edu.co (L. Tirado-Mejía), heariza@uniquindio.edu.co (H. Ariza-Calderón), hriascos@utp.edu.co (H. Riascos), francisco.deanda@gmail.com (F. de Anda), edgar.mosquera@correounivalle.edu.co (E. Mosquera).



Contents lists available at ScienceDirect

Materials Science in Semiconductor Processing

journal homepage: <http://www.elsevier.com/locate/mssp>

Critical thickness as a function of the indium molar fraction in cubic $\text{In}_x\text{Ga}_{1-x}\text{N}$ and the influence in the growth of nanostructures

V.D. Compeán-García^{a,*}, O. Hernández-Vázquez^b, S.A. García-Hernández^b, E.López Luna^b, M. A. Vidal^b

^a CONACyT-Coordinación para la Innovación y Aplicación de la Ciencia y Tecnología (CIACyT), Universidad Autónoma de San Luis Potosí (UASLP), Álvaro Obregón 64, San Luis Potosí, SLP78000, Mexico

^b Coordinación para la Innovación y Aplicación de la Ciencia y Tecnología (CIACyT), Universidad Autónoma de San Luis Potosí (UASLP), Álvaro Obregón 64, San Luis Potosí, SLP78000, Mexico

ARTICLE INFO

Keywords:

$\text{In}_x\text{Ga}_{1-x}\text{N}$
Cubic GaN
Critical thickness
III-Nitrides
 $\beta\text{-In}_x\text{Ga}_{1-x}\text{N}$ nanostructures

ABSTRACT

The critical thickness for the relaxation of cubic (β) $\text{In}_x\text{Ga}_{1-x}\text{N}$ layers grown over (002) $\beta\text{-GaN/MgO}$, with different indium content, particularly of 17, 44, and 70% have been determined experimentally. The layers were grown by plasma-assisted molecular beam epitaxy. In all the samples studied, the critical thickness (h_c) of the pseudomorphic layer was measured with a frame-by-frame analysis of reflection high energy electron diffraction (RHEED) patterns. The growth mode transition during layer growth was identified via RHEED patterns, from layer by layer or 2D to 3D growth mode by gradually transitioning from a streaky to a spotty pattern. The experimental h_c value of $\beta\text{-In}_x\text{Ga}_{1-x}\text{N}$ on $\beta\text{-GaN}$ was compared to values calculated from the Fisher model. For the indium concentration of $x = 0.44$, the self-assembling epitaxial nanostructures were successfully grown in the Stranski–Krastranov growth mode with a critical thickness of 1.8 ± 0.7 nm. The $\beta\text{-In}_{0.44}\text{Ga}_{0.56}\text{N}$ nanostructures showed a variation in morphology and density depending on the deposition time; self-assembled nanodots and nano-bars were confirmed by atomic force microscopy. Photoluminescence spectra of $\beta\text{-In}_{0.44}\text{Ga}_{0.56}\text{N}$ nanostructures showed emissions associated with quantum confinement; these peaks indicate a blue shift with respect to the bulk.

X-ray Photoelectron Spectroscopy results indicate the presence of nitrogen, indium, and gallium on the obtained samples. Also, the intensity dependence with the take-off angle shows weak indium segregation in $\beta\text{-In}_x\text{Ga}_{1-x}\text{N}$ nanostructures.

1. Introduction

In the last two decades, the study of the metastable zinc blende III-Nitrides has increased in importance due to its advantages with respect to wurtzite natural crystallization [1–12]. Higher crystalline symmetry of cubic nitrides compared with hexagonal phase results in material isotropic properties and lack of spontaneous polarization induced-electric fields in the direction parallel to the c -axis. For these reasons, it is expected that cubic III-Nitrides have advantageous properties with respect to the hexagonal phase. In addition, since the $\beta\text{-GaN}$ has a 200 meV lower bandgap than the hexagonal phase, $\beta\text{-In}_x\text{Ga}_{1-x}\text{N}$ requires less indium content to enable the band gap in the visible region

[2–9]; therefore, extending the feasibility of band gap engineering based on III-Nitride semiconductors and converting this alloy in a promising and strategic material in the application of optoelectronics and electronics devices [10,13,14].

However, the growth of $\beta\text{-In}_x\text{Ga}_{1-x}\text{N}$ still has some challenges; one disadvantage of such heterostructures is the reported 9.9% lattice mismatch between $\beta\text{-GaN}$ and $\beta\text{-InN}$ that give rise to high levels of elastic strains. As the layer of $\beta\text{-In}_x\text{Ga}_{1-x}\text{N}$ growth proceeds on $\beta\text{-GaN}$, the increase in stored elastic energy initiates strain relaxation. The relaxation occurs beyond a critical thickness (h_c) either elastically by metamorphic growth mode (2D–3D transition) or plastically by dislocation in the first monolayers [15].

On the other hand. The lattice mismatch provides an opportunity of strain-induced self-assembling epitaxial quantum structures with the layer-plus-island or Stransky-Krastranov (SK) growth mode [16–18].

The inclusion of semiconductor nanostructures grown at the scale where quantum electron confinement effects have a predominant role

* Corresponding author.

E-mail address: damiancompean@gmail.com (V.D. Compeán-García).

<https://doi.org/10.1016/j.mssp.2020.105101>

Received 22 August 2019; Received in revised form 23 March 2020; Accepted 25 March 2020

Available online 7 April 2020

1369-8001/© 2020 Elsevier Ltd. All rights reserved.



Effect of aliphatic chain in dicarboxylic acids on non-isothermal crystallization and mechanical behavior of titanium dioxide/iPP composites



V. Gonzalez-Rodriguez^a, V. Escobar-Barrios^a, M.G. Peña-Juárez^b, E. Pérez^{c,*},
J.A. Gonzalez-Calderon^{d,*}

^a Departamento de Materiales Avanzados, Instituto Potosino de Investigación Científica y Tecnológica (IPICYT), 78216, San Luis Potosí, SLP, Mexico

^b Doctorado Institucional en Ingeniería y Ciencia de Materiales, Universidad Autónoma de San Luis Potosí, Sierra Leona No. 550 Col. Lomas 2da. Sección, 78210, San Luis Potosí, SLP, Mexico

^c Instituto de Física, Universidad Autónoma de San Luis Potosí, Av. Manuel Nava #64, Zona Universitaria, 78290, San Luis Potosí, SLP, Mexico

^d Cátedras CONACYT - Instituto de Física, Universidad Autónoma de San Luis Potosí, Av. Manuel Nava #64, Zona Universitaria, 78290, San Luis Potosí, SLP, Mexico

ARTICLE INFO

Keywords:

Polymer composites
Crystallization
Dicarboxylic acids
Polypropylene
Titanium dioxide

ABSTRACT

Non-isothermal crystallization kinetics of isotactic polypropylene (iPP) and its composites prepared with functionalized titanium dioxide (TiO₂) were investigated by varying both heating rate and dosage of functionalized particles. Jeziorny's and Mo's methods were used to describe the non-isothermal crystallization process. The behavior of crystallization activation energy as a function of the crystallinity degree was evaluated by applying an isoconversional method. The modification of the TiO₂ surface was done by testing three different carboxylic acids: glutaric, pimelic and azelaic acid and these particles were tested at different concentrations in iPP, 0.1, 0.5 and 1 % w/w; which had a high effect on the crystallization process of the polymer matrix. It was demonstrated the efficiency of the dry basis chemical reaction as a method to modify with dicarboxylic acids the surface of TiO₂ particles. Such organic coatings chemically bonded to the surface of the TiO₂ promoted a better incorporation of the iPP chains during crystallization and there is a clear effect of the length of dicarboxylic acids since the acids with more carbons, pimelic and azelaic, decreased the time to reach the crystalline state. Besides, the values of Young's modulus were modified by functionalized TiO₂ particles, being the acid with the longest chain (azelaic acid) the one that more increased this parameter.

1. Introduction

Polypropylene is a linear hydrocarbon polymer widely used in industry. It is used in a variety of applications that include the packaging of consumer products and parts for various industries such as automotive and textiles. Polypropylene is practically inert, highly recyclable, has no toxic by-products when it is incinerated, and has low production costs [1]. This thermoplastic is manufactured by polymerization that combines propylene monomers to form long chains. A monomer reacts with a metallocene-type catalyst to generate a reactive site that may promote the subsequent addition of monomers in propylene unsaturations [2–9]. There are three types of propylene structures depending on their molecular arrangement: isotactic polypropylene (iPP), syndiotactic polypropylene (sPP) and atactic polypropylene (aPP). iPP, which has all its methyl groups on the same side of the chain, is the most common and interesting structure to study. It is a polycrystalline olefin with different degrees and types of crystallinity depending on processing,

crystallization conditions or additives used. This type of semicrystalline polymer generally has high strength and stiffness [10]. Crystallization is carried out when the material is conveyed to the solidification point or when the solvent evaporates from the matrix. In most cases, materials present not only crystalline regions but also amorphous in the polymeric structure. Polymer chains are arranged as lamellae with union centers among them since polymer chains are of enormous lengths, these enter and leave the lamellae interconnecting with neighboring lamellae to form the large crystalline arrangement. The union centers provide the material with flexibility and resistance to impact [10]. The lamella growth can be carried out spontaneously by cooling the material or by inserting particles that act as nucleation sites, these fillers can be either organic compounds or metal oxides [10,11]. There are α , β , and γ polypropylene arrangements. The α arrangement is the innate and most frequent form in iPP matrices; made under normal processing conditions, it consists of a helical structure in a monoclinic unit cell [2,12], which shows a growth identified as malt cross [4,10]. The β form, with a

* Corresponding authors.

E-mail addresses: elias@ifisica.uaslp.mx (E. Pérez), amir@ifisica.uaslp.mx (J.A. Gonzalez-Calderon).

<https://doi.org/10.1016/j.tca.2020.178543>

Received 21 August 2019; Received in revised form 28 January 2020; Accepted 3 February 2020

Available online 04 February 2020

0040-6031/ © 2020 Elsevier B.V. All rights reserved.



Elastic modulus and hardness of cubic GaN grown by molecular beam epitaxy obtained by nanoindentation

S.A. García Hernández^a, V.D. Compeán García^b, E. López Luna^a, M.A. Vidal^{a,*}

^a *Coordinación para la Innovación y la Aplicación de la Ciencia y la Tecnología (CIACYT), Universidad Autónoma de San Luis Potosí, Álvaro Obregón 64, 78000 San Luis Potosí, S.L.P., México*

^b *CONACYT—Coordinación para la Innovación y la Aplicación de la Ciencia y la Tecnología (CIACYT), Universidad Autónoma de San Luis Potosí, Álvaro Obregón 64, 78000 San Luis Potosí, S.L.P., México*

ARTICLE INFO

Keywords:

Cubic gallium nitride
Plasma-assisted molecular beam epitaxy
Mechanical properties
Berkovich indentation
Young's modulus
Thin films

ABSTRACT

The mechanical properties of gallium nitride thin films in the cubic phase (c-GaN) measured by Berkovich nanoindentation are reported here. The c-GaN thin films were grown on MgO (100) substrates by plasma-assisted molecular beam epitaxy. The X-ray diffraction results show that GaN thin films correspond to more than 99% cubic phase in all cases. Plastic transitions called pop-in events are observed during loading in some load-displacement curves at different depths. We believe that pop-in event is present when the tip interacts with defects encountered at different depths. The mean values of the hardness and Young's modulus of cubic GaN are 22 ± 1 GPa, and 293 ± 12 , respectively.

1. Introduction

In the last few decades, thin films of III-Nitrides semiconductors have been used to fabricate electronic and optoelectronic devices [1–3]. For instance, some of the most significant applications are solid-state lighting, tandem solar cells, high-power, and high-frequency transistors, among other devices [2,4–6]. Most of their potential in these fields is due to the significant modulation of their properties with alloy composition. Under conditions of thermodynamic equilibrium, the crystal growth of III-Nitrides compounds has a hexagonal phase. Nevertheless, by slightly varying in the growth parameters, the non-equilibrium cubic phase can be obtained.

The higher crystalline symmetry of the cubic III-Nitrides concerning the hexagonal phase results in more isotropic properties. Besides, it is free of spontaneous polarization induced-electric fields in the direction parallel to the c-axis. It is expected for cubic III-Nitrides advantages to respect hexagonal phases, such as superior electronic properties, higher carrier mobilities, higher drift velocities, better doping efficiencies and cleavage planes [7,8].

Since this significant breakthrough, the development of methods to improve growing conditions of III-Nitride films in the scale of nanometers has brought remarkable results in electronic and optoelectronic devices, and high-precision diagnostic techniques to analyze such films have been developed. Therefore, it is crucial to carry out systematic studies of the mechanical properties of these thin-film materials. One of

the promising diagnostic methods to study the mechanical properties of thin films and their crystalline quality is nanoindentation.

There are limited studies of the mechanical properties of the h-III-Nitrides and even fewer studies regarding the cubic phase. Pezoldt et al. [9] studied the mechanical properties of cubic GaN thin films with a Vickers tip. As is known, the mechanical properties like hardness differ with Vickers and Berkovich tip, as indicated in this reference [10,11], where the Vickers tip is commonly used for bulk materials. The most widely and currently used technique in thin films is nanoindentation with a Berkovich tip.

Nanoindentation has been established as an improved method for precise determination (within 5% error) of the mechanical properties of thin films [12–15] such as hardness and the elastic modulus from the load-displacement data obtained from nanoindentation experiments [16]. A Berkovich diamond indenter is most used in nanoindentation tests because it is easier to make its sides converge at a point sharper [17] than a Vickers indenter, thus providing high precision in the indentation process.

The analysis of the load-displacement curves obtained during the nanoindentation allows the determination of hardness and elastic modulus of the material following the Oliver and Pharr method [16,18]. Among the typical mechanical properties of interest, such as hardness and elastic modulus, the details obtained from the indentation test can also give insight into the behavior associated with the on-set of plastic deformation or fracture.

* Corresponding author.

E-mail address: mavidalborbolla@yahoo.com.mx (M.A. Vidal).

Many-electron redistribution in n -doped semiconductor nanostructures under external electric field by using a center-of-mass approach

Reyna Méndez-Camacho,^{1,2,*} Ramón Castañeda-Priego¹, and Esteban Cruz-Hernández^{2,†}

¹*División de Ciencias e Ingenierías, Campus León, Universidad de Guanajuato, Loma del Bosque 103, 37150 León, México*

²*Coordinación para la Innovación y Aplicación de la Ciencia y la Tecnología, Universidad Autónoma de San Luis Potosí, Sierra Leona 550, 78210 San Luis Potosí, México*



(Received 19 April 2020; revised 13 June 2020; accepted 16 June 2020; published 1 July 2020)

The study of an external force triggering the many-electron redistribution in nanostructures is of importance for both theoretical and practical interest in condensed matter physics. Hence, the goal of this contribution is to theoretically investigate the influence of an external electric field (EEF) on the ground and excited states of a system of many-electrons confined in GaAs/AlGaAs nanostructures. To deal with the many-body issue, we employ a Yukawa-like potential in a two-electron framework, while it is proposed to explore the challenging EEF contribution by analyzing its effect on the electronic center-of-mass framework. Thus, while the Yukawa-like potential allows us to model the many-electron interaction in the range from 10^{17} to 10^{23} electrons/cm³, via the adjustment of a simple screening parameter; the center-of-mass approximation also allows us to describe easily the effect of the EEF separately. Internal electronic distributions in nanostructures of various sizes and electronic concentrations are obtained and discussed for EEF of variable magnitude. This alternative approach enables us to decouple the electron-electron and the EEF interactions, which is useful in determining the origin of the observed features. We show that this theoretical framework is well suited to get relevant information in semiconductor nanostructures of practical sizes and realistic doped levels.

DOI: [10.1103/PhysRevB.102.035403](https://doi.org/10.1103/PhysRevB.102.035403)

I. INTRODUCTION

Recent advances in nanofabrication and the technology of semiconductor nanostructures, such as quantum wires (QWRs) or quantum dots (QDs) [1–3], promise a wide spectrum of potential applications. The latter are possible due to the deep modification of the nanostructure physical properties, such as sharp density of states, ballistic electronic transport, or enriched optical properties that are quite different to those of the bulk material [3,4].

In particular, because QWRs possess both transversal quantum confinement and longitudinal ballistic transport, extensive experimental and theoretical studies [5–8] have shown their high potential to be applied in the next generation of optoelectronic and electronic devices [9–12]. In most of the nanostructure-based devices, the activation of such properties involves the application of an external voltage (V_{ext}), which in turn produces an EEF (E_{ext}). It is then crucial to deeply understand its impact on the internal electronic reconfiguration and the related modification on the QWRs and QDs properties.

Due to the issues related to the modeling of large (micrometric) wires and high electronic concentrations (around 10^{17} electrons/cm³), most of the reported works address the study of an EEF on semiconductor nanostructures of small (nanometric) size, containing just one or a few electrons.

So, when addressing QWRs, usually a transverse EEF is applied (along the short, nanometric, QWR cross-section) and single electronic or excitons redistribution, known as the Stark effect, are usually reported [13–19]. For example, for semiconductor QDs an electronic Stark shift (in the opposite direction to the EEF and towards lower energies), changes in the photoluminescence emission and optical absorption have been reported [17,18,20]. However, the most common configuration, when the EEF is applied along the wire remains much less studied mainly because it implies dealing with relatively large sizes and many-body electron-electron (e - e) interactions, which is a quite challenging issue.

In recent publications, we proposed the use of a Yukawa-like-interaction to deal with the many-body problem, which allows us to describe the e - e interaction in n -doped semiconductor nanostructures of typical electronic concentrations and realistic lengths [21,22]. By using this formalism, for example, valuable information about the Wigner molecule formation in QWRs, such as critical electronic-densities or optimal geometries were reported for different semiconductor materials. In the present work, we study the effect of an E_{ext} on the electronic distribution in semiconductor GaAs/AlGaAs nanostructures. To this end, the e - e is handled as in Ref. [22] while the E_{ext} is decoupled by applying it to the electronic center-of-mass framework of the entire e - e interacting system.

Hereafter, we solve the Schrödinger equation by decoupling the e - e relative framework from the center-of-mass one of the total electronic distribution. In the two-electron framework, two nonrelativistic electrons in GaAs wells

*reyna.mendez@uaslp.mx

†esteban.cruz@uaslp.mx

Potential of Mean Force Calculations for an S_N2 Fluorination Reaction in Five Different Imidazolium Ionic Liquid Solvents Using Quantum Mechanics/Molecular Mechanics Molecular Dynamics Simulations

Joel Sánchez-Badillo, Marco Gallo,* Ricardo A. Guirado-López, and Raúl González-García



Cite This: <https://dx.doi.org/10.1021/acs.jpcc.0c03192>



Read Online

ACCESS |



Metrics & More

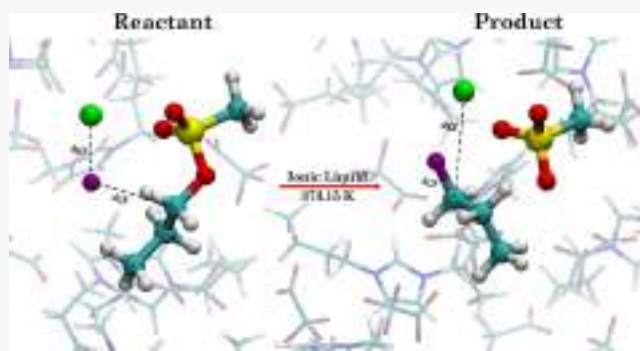


Article Recommendations



Supporting Information

ABSTRACT: The use of ionic liquids (ILs) as both catalysts and solvents in a wide range of chemical reactions has received considerable attention over the last few years due to their positive effects in enhancing reaction rates and selectivities. In this work, hybrid quantum mechanics/molecular mechanics (QM/MM) molecular dynamics simulations were carried out in conjunction with umbrella-sampling techniques to study the bimolecular nucleophilic substitution (S_N2) fluorination reaction between propyl-mesylate and potassium fluoride using five ILs as solvents, specifically, 1-butyl-3-methylimidazolium mesylate ($[C_4mim][OMs]$), 1-butyl-3-methylimidazolium tetrafluoroborate ($[C_4mim][BF_4]$), 1-butyl-3-methylimidazolium trifluoroacetate ($[C_4mim][CF_3COO]$), 1-butyl-3-methylimidazolium bromide ($[C_4mim][Br]$), and 1-butyl-3-methylimidazolium chloride ($[C_4mim][Cl]$) at 373.15 K. The QM region (reactive part) in all QM/MM systems was simulated using the Parametric Method 6 (PM6) semiempirical methods, and for the MM region (IL solvent), classical force fields (FF) were employed, with the FF developed within the group. The calculated activation free energy barriers (ΔG^\ddagger) for the S_N2 reaction in the presence of $[C_4mim][OMs]$ and $[C_4mim][BF_4]$ ILs were in agreement with the experimental values reported in the literature. On the other hand, only predicted values were obtained for the activation energies for the $[C_4mim][CF_3COO]$, $[C_4mim][Br]$, and $[C_4mim][Cl]$ ILs. These activation energies indicated that the S_N2 reaction would be more facile to proceed using the $[C_4mim][Cl]$ and $[C_4mim][OMs]$ ILs, in contrast with the use of $[C_4mim][Br]$ IL, which presented the highest activation energy. Energy-pair distributions, radial distribution functions, and noncovalent interactions (NCI) were also calculated to elucidate the molecular interactions between the reactive QM region and the solvents or reaction media. From these calculations, it was found that not only the reactivity can be enhanced by selecting a specific anion to increase the K–F separation but also the cation plays a relevant role, producing a synergetic effect by forming hydrogen bonds with the fluorine atom from KF and with the oxygen atoms within the mesylate leaving group. Three interactions are significant for the IL catalytic behavior, $F_{QM}-HX$, $K_{QM}-anion$, and $O_{QM}-HX$ interactions, where the F_{QM} and K_{QM} labels correspond to fluorine and potassium atoms from the KF salt, O_{QM} corresponds to oxygen atoms within the mesylate leaving group (reactant), and HX refers to hydrogen atoms within the IL cation. The NCI analysis revealed that $K_{QM}-anion$ interactions are of weak type, indicating the importance of hydrogen bond interactions from the cation such as $F_{QM}-HX$ and $O_{QM}-HX$ for the catalytic behavior of ILs.



INTRODUCTION

Ionic liquids (ILs) are chemical compounds composed of oppositely charged ions, i.e., cations and anions; however, unlike common molten or fused salts, ILs are liquids at temperatures below 100 °C.^{1,2} This liquid state is favored from the bulky asymmetry of its ions, making their packing difficult.^{1,3,4} Selecting or modifying the nature of the cation in the IL has an effect on its viscosity,^{5,6} melting point,^{7,8} performance as a reaction medium,⁹ and gas solubility in a small degree,^{6,10} whereas the modification of the anion in IL has a large effect on gas solubility,^{10,11} decomposition

temperature,⁷ and catalytic capacity.¹² By combining different cations and anions, it is possible to produce ILs with different properties such as low vapor pressure,^{13,14} a wide range of thermal stabilities,^{7,15,16} densities,^{7,12} gas solubilities,^{10,12}

Received: April 9, 2020

Published: April 30, 2020

Electronic Circular Dichroism of Fullerenols

J. Cornejo-Jacob, J. Vicente-Santiago, and R. A. Guirado-López*

Cite This: *J. Phys. Chem. C* 2020, 124, 7458–7466

Read Online

ACCESS |



Metrics & More

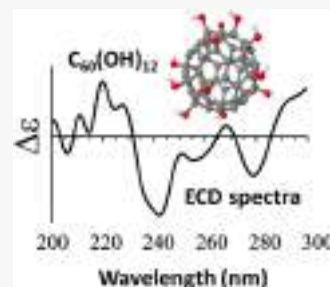


Article Recommendations



Supporting Information

ABSTRACT: We present extensive time-dependent density functional theory calculations dedicated to analyzing the optical properties of model low-hydroxylated $C_{60}(OH)_{12}$ fullerenols. In all our considered isomers, the simulated UV–vis spectra show similar features having in general two well-defined absorption maxima approximately located at 220 and 300 nm. In addition, we calculate, for the first time, the electronic circular dichroism (ECD) spectra of $C_{60}(OH)_{12}$ fullerenols. We obtain that the adsorption of OH groups on the C_{60} surface can reduce the symmetry of the molecular complex, resulting in the appearance of notable optical activity in these kinds of carbon nanostructures made of achiral components. The here-predicted ECD spectra strongly depend on the structure of the OH overlayer, extends from the ultraviolet to the infrared regions, and shows precise features than can be used to distinguish the presence of specific $C_{60}(OH)_{12}$ isomers in a sample. We conclude that in the case of low hydroxylated fullerenols, chirality can be induced by modifying the adsorbed configuration of the OH groups, providing thus novel biological applications for these carbon compounds. We hope our results could motivate optical activity experiments on these kinds of systems.



1. INTRODUCTION

In the last years, it has been clearly established that the properties of C_{60} fullerenes can be strongly altered by the chemical functionalization of its surface.^{1–5} This type of organic derivatives has been found to play an important role in material science,^{6–8} as well as for realizing biomedical^{9–12} and catalytic^{13–15} applications where the solubility and the charge density distribution are key variables to achieve their optimal functionality. In particular, hydroxylated fullerenes^{9–12,15,16} have been the subject of intense research in the last decade since they can be synthesized by various (and relatively easy) experimental techniques. Clearly, different fabrication procedures can lead to the formation of C_{60} cages covered with OH groups adopting various adsorbed phases, which are currently unknown. This is important to emphasize since the properties of $C_{60}(OH)_x$ fullerenols are expected to strongly depend on the amount and distribution of the hydroxyl species. In this respect, extensive experimental characterization has been performed employing Fourier transform infrared spectroscopy (FTIR),¹⁷ transmission electron microscopy (TEM),^{9–11} dynamic light scattering (DLS),¹⁸ and X-ray photoelectron spectroscopy (XPS)^{17,19} in condensed, liquid, and gas phases, and important aspects related to their structure, chemical composition, and aggregation behavior have been revealed.

However, despite the intense research activity mentioned above, it is important to emphasize that none of the previous experimental methods can provide us with the absolute atomic configuration of these complex (sub-nanometer sized) fullerene systems, information that is of fundamental importance to understand the observed macroscopic behavior. Consequently, it is necessary to consider the use of additional spectroscopic techniques that can allow us to obtain structural

information that goes beyond the actual experimental evidence. In this respect, optical spectroscopy could play a fundamental role since the optical response of a molecule and its molecular (and electronic) structure are strongly correlated. Here, it is important to emphasize that even if measurements of the UV–vis spectra of different fullerene complexes typically look very similar, this is not the case for the electronic circular dichroism (ECD) spectra of the samples.^{20–23} As is well known, the ECD detects small differences in the UV–vis spectra between right and left circularly polarized light, is more detailed and structured, and is more sensitive to the composition and local atomic environment of the molecules. Actually, fullerene complexes with very similar structure can produce contrasting spectral patterns in the CD signals, providing thus a possibility for their identification by analyzing the sign and intensity of the Cotton effect at a specific nanometer range.^{24–27}

The possible appearance of the optical activity in fullerenols is relevant to analyze since some of its molecular properties are expected to be altered by chirality. This is particularly important in the field of biology (where chiral molecules are highly abundant in living creatures) since several studies have shown interesting activity in photodynamic therapy^{28–30} and neuroprotection^{31,32} for these compounds. Furthermore, chiral recognition applications as well as the development of highly

Received: December 19, 2019

Revised: March 9, 2020

Published: March 12, 2020



Infrared thermography of abdominal wall in acute appendicitis: Proof of concept study

Jose Luis Ramirez-GarciaLuna^{a,b}, Luis Roberto Vera-Bañuelos^c, Lorenzo Guevara-Torres^c,
Mario Aurelio Martínez-Jiménez^{b,c,d}, Alejandra Ortiz-Dosal^{d,e}, Francisco Javier Gonzalez^{d,e},
Eleazar Samuel Kolosovas-Machuca^{d,e,*}

^a Division of Experimental Surgery, Faculty of Medicine, McGill University, 3605 Rue de la Montagne, H3G 2M1 Montréal, QC, Canada

^b Department of Surgery, Faculty of Medicine, Universidad Autónoma de San Luis Potosí, 2405 Venustiano Carranza Ave., 78210 San Luis Potosí, SLP, Mexico

^c Department of Surgery, Hospital Central Dr. Ignacio Morones Prieto, Zona Universitaria, 78290 San Luis Potosí, SLP, Mexico

^d Doctorado Institucional en Ingeniería y Ciencia de Materiales (DICIM-UASLP), Universidad Autónoma de San Luis Potosí, 550 Sierra Leona Ave, 78210 San Luis Potosí, SLP, Mexico

^e Coordinación para la Innovación y Aplicación de la Ciencia y la Tecnología, Universidad Autónoma de San Luis Potosí, 550 Sierra Leona Ave, 78210 San Luis Potosí, SLP, Mexico

ARTICLE INFO

Keywords:

Appendicitis
Acute abdomen
Infrared imaging
Machine learning

ABSTRACT

Objective: Diagnosis of acute appendicitis may be challenging. The current imaging methods have modest sensitivities and specificities. This study aimed to evaluate skin infrared thermal (IRT) imaging as a diagnostic adjunct for acute appendicitis in adults.

Methods: We conducted a prospective observational study in 51 patients with appendicitis, 20

with abdominal pain (no appendicitis) and 51 healthy controls. Temperature of the skin overlying abdominal lower quadrants, right (RLQ) and left (LLQ), were recorded and compared between groups. Using a machine learning algorithm, we identified which parameters discriminated between groups and compared the diagnostic accuracy of IRT to the final diagnosis.

Results: RLQ temperature > 34 °C discriminate healthy controls and patients with acute abdomen; a delta > 0.35 °C in RLQ vs LLQ discriminate patients with and without appendicitis. Compared to the ultrasound-based diagnosis, IRT has a sensitivity of 91% and a specificity of 56% to diagnose appendicitis.

Conclusions: IRT could be an adjunct tool in the diagnosis of appendicitis in settings with limited resources. Further research is needed to confirm and translate our results into clinical practice.

1. Introduction

Acute appendicitis has an estimated lifetime risk of approximately 7% and is one of the most common causes of acute abdomen, defined as the acute onset of pain caused by a potentially life-threatening intra-abdominal pathology that requires urgent surgical intervention [1–3]. This diagnosis remains challenging because its clinical presentation can be atypical and symptoms often overlap with other conditions that may or may not need surgical treatment. Because reported symptoms may vary according to anatomic position of the appendix, some of the conditions that could mimic acute appendicitis are right-sided colonic diverticulitis, segmental omental infarction, urolithiasis, infectious ileocolitis, hemorrhagic ovarian cyst, mesenteric adenitis, Crohn

disease, acute pyelonephritis, colonic malignancy, ovarian torsion, mesenteric ischemia, Meckel diverticulitis, rupture of ectopic pregnancy, pelvic inflammatory disease, among others [4]. The classical signs and symptoms of acute appendicitis, such as a history of abdominal pain that begins in the central abdomen and migrates to the right lower quadrant, tenderness to palpation on physical examination, nausea or vomiting, mild leukocytosis, and low-grade fever, are only present in approximately 50% of the patients [5]. Thus, the clinical examination has a poor predictive value, even when signs and symptoms are used in combination. Biomarkers such as leukocyte count and C-reactive protein are used to complete the clinical picture, especially when the diagnosis is obscure, but they are non-specific. Imaging adjuncts, such as ultrasonography or computed tomography (CT) even

* Corresponding author at: Coordinación para la Innovación y Aplicación de la Ciencia y la Tecnología, Universidad Autónoma de San Luis Potosí, San Luis Potosí, SLP, México. Av. Sierra Leona #550, Col. Lomas 2a., 78210 San Luis, SLP, Mexico.

E-mail address: samuel.kolosovas@uaslp.mx (E.S. Kolosovas-Machuca).

<https://doi.org/10.1016/j.infrared.2019.103165>

Received 17 October 2019; Received in revised form 20 December 2019; Accepted 20 December 2019

Available online 23 December 2019

1350-4495/ © 2019 Elsevier B.V. All rights reserved.



Physical characterization of sunflower seeds dehydrated by using electromagnetic induction and low-pressure system



Arturo Agustin Ortiz-Hernandez^a, Ma. Araiza-Esquivel^{b,*}, Lucia Delgadillo-Ruiz^c, Jose Juan Ortega-Sigala^d, Hector Antonio Durán-Muñoz^e, Victor Hugo Mendez-Garcia^f, Miguel Jose Yacaman^g, Hector Rene Vega-Carrillo^h

^a AORTech, Research Department & Coordinación de Ingeniería Mecatrónica, Universidad Politécnica de Zacatecas, Mexico

^b Unidad Académica de Ingeniería Eléctrica, Universidad Autónoma de Zacatecas, Mexico

^c Unidad Académica de Biología, Universidad Autónoma de Zacatecas, Mexico

^d Unidad Académica de Física, Universidad Autónoma de Zacatecas, Mexico

^e Coordinación de Ingeniería Industrial, Universidad Politécnica de Zacatecas, Mexico

^f Coordinación para la Innovación y Aplicación de la Ciencia y la Tecnología, Universidad Autónoma de San Luis Potosí

^g Physics & Astronomy, University of Texas at San Antonio, Mexico

^h Unidad Académica de Estudios Nucleares, Mexico

ARTICLE INFO

Keywords:

Dehydration
Electromagnetic induction
Low pressure
Sunflower seeds
Physical characterization

ABSTRACT

Drying is a widely used food preservation process in which water removal minimizes much of the moisture that causes deterioration reactions that impact the bioproduct quality. The objects of studying are high oleic sunflower seeds which are recognized as a worldwide source of edible oil; consequently, they have significant importance on health and food security. This work presents part of the results of a systematic study to compare the affectations on the several physical parameters of sunflower seeds and kernels with the Thermo-Solar Dehydration method (TSD) compared to Dehydration with Electromagnetic Induction at Low Pressures (DEMI-LP), finding that the in the last one the time to reach the 8% of the total moisture content was 2.5 times shorter, interesting physical effects and an increment of 5% in the volumetric expansion coefficient, reflected in a reduction of the cut resistance (Dehull) of 0.5KgF significant advantages for the food drying industry.

1. Introduction

According to the Department of Agriculture and Food (FAO) of the of United Nations (UN) during the projection period 2016–2025, world agricultural production of cereals and oilseeds for the production of vegetable oil (including sunflower seed) will be expanded, if natural conditions favor it. Additionally, an annual growth of 1.5% is expected due to the growing demand for biofuels from vegetable oils as a result of the continuous compliance with mandatory regulations for the use of biodiesel (OCDE-FAO, 2016).

In 2016, the world production of *Helianthus annuus*, whose common name is sunflower, was 45.75 million Tons. The major producing countries were Ukraine 30.6%, Russia 24.0%, Argentina 7.4%, and China 6.2%. Mexico only contributed with 0.28% of production, and the area destined for this crop has had a considerable increase going

from 54 ha in 2000 to 7,216.72 ha in 2018 (Krautgartner, Lefebvre, Rehder, Boshnakova, & EU, 2018).

The sunflower (*Helianthus annuus*) is one of the world's leading oilseed crops, second only to soybean for the total high oleic oil production (Pighinelli, Ferrari, Miguel, & Park, 2011). Here lies its importance and its physical characteristic that allows the design and development of specialized equipment with the capacity for drying, handling, separating, dehulling, and storing systems (Acevedo Picon, Jaime, & Gelvez Figueredo, 2007).

The specific physical properties after dehydration of sunflower seeds which would be useful for the design of the dehulling process depend on surfaces, sphericity, and storage systems (Gupta, Arora, & Sharma, 2006; Gupta & Das, 1997; Pérez, Bäumlner, Crapiste, & Carelli, 2019; Perez, Crapiste, & Carelli, 2007). A variety of physical properties of the sunflower species that originated in Mesoamerica (Alvarado,

* Corresponding author.

E-mail addresses: aaortizhernandez@upz.edu.mx (A.A. Ortiz-Hernandez), araizama@uaz.edu.mx (M. Araiza-Esquivel), luciadeldgadillo@uaz.edu.mx (L. Delgadillo-Ruiz), jjosila@fisica.uaz.edu.mx (J.J. Ortega-Sigala), hduran@upz.edu.mx (H.A. Durán-Muñoz), victor.mendez@uaslp.mx (V.H. Mendez-Garcia), miguel.yacaman@utsa.edu (M.J. Yacaman), rvega@uaz.edu.mx (H.R. Vega-Carrillo).

<https://doi.org/10.1016/j.ifset.2019.102285>

Received 21 July 2019; Received in revised form 27 December 2019; Accepted 27 December 2019

Available online 18 January 2020

1466-8564/ © 2020 Elsevier Ltd. All rights reserved.